JOURNAL OF PETROLOGY | VOLUME 51 | NUMBER 7 | PAGES 1571–1595 | 2010 | doi:10.1093/petrology/egq030

Two Contrasting H_2O-rich Components in Primary Melt Inclusions from Mount Shasta

M. LE VOYER[1]*, E. F. ROSE-KOGA[1], N. SHIMIZU[2], T. L. GROVE[3] AND P. SCHIANO[1]

[1]LABORATOIRE MAGMAS ET VOLCANS–CNRS-UBP-IRD, 63000 CLERMONT-FERRAND, FRANCE

[2]WOODS HOLE OCEANOGRAPHIC INSTITUTION, WOODS HOLE, MA 02543, USA

[3]MIT, DEPARTMENT OF EARTH, ATMOSPHERIC AND PLANETARY SCIENCES, CAMBRIDGE, MA 02139, USA

RECEIVED JULY 20, 2009; ACCEPTED MAY 10, 2010

In addition to the abundant andesite and dacite lavas of the Mt. Shasta stratocone, primitive mafic lavas have erupted during the Quaternary from the Mt. Shasta region. Two types of basic lavas are the focus of this study: nearly anhydrous high-aluminium olivine tholeiites, produced by decompression melting, and basaltic andesites, produced by melting of a metasomatized mantle source (i.e. modified by various amounts of H_2O-rich components). Here we provide further insight into the origin and the coexistence of these two types of magma based on a detailed study of the dissolved volatile contents in melt inclusions trapped in magnesium-rich olivine crystals from both tholeiites and basaltic andesites. The melt inclusions fall on the primitive extension of their respective host lava compositions: (1) the tholeiite melt inclusions are nearly anhydrous melts with low and clustered volatiles compositions; (2) the basaltic andesite melt inclusions are 'wet' melts with higher and more variable volatile contents (up to 2·6 wt% H_2O, 820 ppm CO_2, 1270 ppm Cl, 1220 ppm F and 6280 ppm S) than those of the tholeiite melt inclusions. The basaltic andesite melt inclusions are enriched in fluid-mobile elements and in incompatible trace elements: they display a stronger signature of slab-derived components than their host lavas. The selective enrichment of the basaltic andesite melt inclusions in fluid-mobile elements such as K, F, Cl, Ba and B as well as their contrasting $\delta^{11}B$ (from $-10{\cdot}2 \pm 1{\cdot}3$‰ to $-3{\cdot}2 \pm 0{\cdot}9$‰ for the melt inclusions from sample 95-15 and from $-4{\cdot}9 \pm 1{\cdot}1$‰ to $+4{\cdot}4 \pm 1{\cdot}1$‰ for the melt inclusions from samples 85-1a and 85-47) show the imprints of two distinct slab-derived components C1 and C2. Using trace element ratios, we modelled the compositions of these two H_2O-rich components (C1 with Cl/F of 1·1 is rich in both in high field strength elements and incompatible trace elements, whereas C2 with Cl/F of 4·0 is poorer in trace elements) and show that they represent mixing between sediment melts and dehydration fluids from the altered oceanic crust.

KEY WORDS: *geochemistry; subduction; arc magmatism; melt inclusions; volatile elements; boron isotopes; Cascades Arc; Mount Shasta*

INTRODUCTION

The Cascades volcanic arc is characterized by subduction of young (12–14 Ma beneath Mt. Shasta; Green & Harry, 1999) oceanic lithosphere of the Juan de Fuca and Gorda plates beneath the North American plate (inset Fig. 1). This subduction has one of the lowest subduction rates observed (40 mm/year; Wilson, 1988). Consequently, the slab undergoes extensive metamorphism and dehydration before reaching sub-arc depths, where the slab-derived flux is expected to be smaller than at typical cool subduction zones such as the Mariana arc (e.g. Leeman *et al.*, 2005). It has been proposed that the Cascades lavas are generated not only by flux melting, as in typical cold subduction zones, but also by decompression melting, resulting thus in the formation of basalts with chemical similarities to intra-plate basalts and a high temperature of melt segregation (e.g. Conrey *et al.*, 1997; Righter, 2000; Leeman *et al.*, 2004, 2005; Smith & Leeman, 2005; Schmidt *et al.*, 2008; Jicha *et al.*, 2009).

*Corresponding author. Present address: MC 100-23, California Institute of Technology, Pasadena, CA 91125, USA. Telephone: 1-626-395-2536. E-mail: mlevoyer@caltech.edu

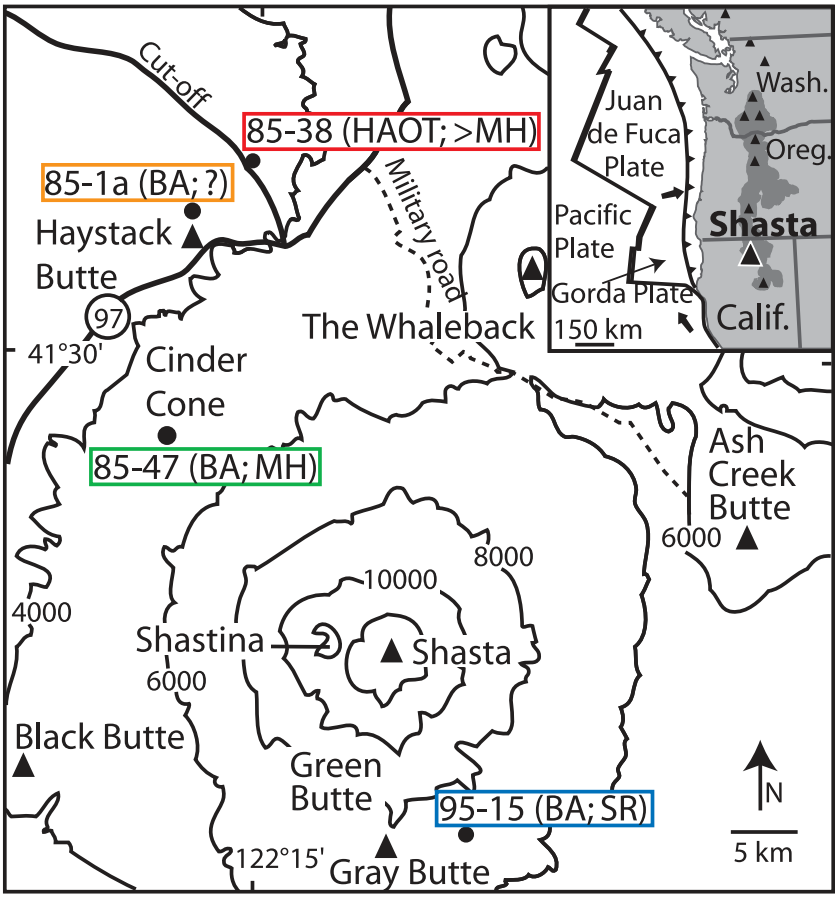

Fig. 1. Sample location map for Mt. Shasta and vicinity (modified from Baker *et al.*, 1994). Contour elevations are given in feet. SR, Sargents Ridge age (<250 to >130 ka BP); MH, Misery Hill age (80–10 ka BP); (?), age unknown (Grove *et al.*, 2002). Inset: schematic tectonic map of the Cascades volcanic arc.

Various mafic lavas have erupted in the vicinity of Mt. Shasta. They belong to three groups: high-aluminium olivine tholeiites (HAOT; also referred to as high-alumina basalts, HAB), basaltic andesites (BA) and primitive magnesium andesites (PMA; Baker *et al.*, 1994; Grove *et al.*, 2002). According to previous studies (Bartels *et al.* 1991; Sisson & Grove, 1993; Baker *et al.*, 1994; Grove *et al.*, 2002), the HAOT derive from decompression melting of a mantle source only insignificantly affected by slab-derived fluids. The BA and the PMA, however, display more variable compositions with a stronger fluid imprint compared with the HAOT. They may represent flux melting of a depleted mantle source with a variable and high water content (3–5 wt% H_2O for the BA, up to 6 wt% for the PMA; Baker *et al.*, 1994; Gaetani *et al.*, 1998; Grove *et al.*, 2002). The origin of the PMA is still under debate: either they represent a nearly primary magma (Grove *et al.*, 2002; Barr *et al.*, 2007, 2008) or they derive from mixing between basic and dacitic end-members combined with contamination with magnesium-rich country rocks (Streck *et al.*, 2007, 2008). This study focuses on the origin of the HAOT and the BA only.

The aims of this study are: (1) to identify the primary magmas of the HAOT and the BA magmatic series at Mt. Shasta using olivine-hosted melt inclusions; (2) to determine their pre-eruptive volatile contents; (3) to discuss the role of the slab component(s) in their generation. To this end, we analyzed the major and trace element compositions, the volatile element contents (H_2O, CO_2, F, Cl and S) and the boron isotope compositions of olivine-hosted melt inclusions from a set of HAOT and BA samples. We show that the melt inclusions from the two groups of mafic lavas have distinct compositions and contrasting pre-eruptive volatile contents: the HAOT melt inclusions have low pre-eruptive volatile contents and represent primitive melts of a volatile-poor mantle source, whereas the BA melt inclusions indicate variable enrichment by slab-derived components of their depleted mantle source. The compositions of the BA melt inclusions allow us to distinguish two H_2O-rich components with contrasting Cl/F and boron isotope concentrations.

GEOLOGICAL SETTING AND SAMPLING

Mt. Shasta (Fig. 1) is an extensively studied stratovolcano located at the southern end of the Cascades chain (e.g. Williams, 1932*a*, 1932*b*, 1934, 1949; Macdonald, 1966; Christiansen *et al.*, 1977; Baker, 1988; Baker *et al.*, 1994; Grove *et al.*, 2002, 2003, 2005; inset Fig. 1). The Mt. Shasta stratocone has erupted over 500 km^3 of andesite and dacite lavas during four episodes of cone building (the oldest is Sargents Ridge, then Misery Hill, Shastina, and finally Hotlum; e.g. Grove *et al.*, 2002). Primitive mafic lavas have also been erupted in the vicinity of Mt. Shasta as cinder cones and lava flows from flank vents (Fig. 1).

We chose four mafic samples from these flank eruptions that have previously been characterized in terms of whole-rock geochemistry: one HAOT sample (85-38) and three BA samples (85-1a, 85-47 and 95-15; Fig. 1). Their major and trace element compositions are reported in Table 1 (for further details, see Baker *et al.*, 1994; Grove *et al.*, 2002). We selected olivine-hosted primary melt inclusions (inclusions randomly distributed in the crystals and showing no sign of leakage; Roedder, 1984) for further study because they represent drops of instantaneous melts that have been formed in thermodynamic equilibrium with their hosts (Schiano, 2003). The selected primary melt inclusions were trapped in polyhedral olivine crystals (i.e. grown at a slow cooling rate) with diameters ranging from 0·4 to 1·5 mm. This olivine morphology prevents us from dealing with melt inclusions affected by the incorporation of boundary layers that form at crystal–liquid interfaces during rapid growth (Faure & Schiano, 2005). The melt inclusions display rounded or ovoid shapes and their size ranges from 20 to 80 μm. Most of them are partially crystallized: they contain various amounts of daughter minerals in a glassy or devitrified matrix. They also enclose (1) a rim of host olivine that crystallized on the inclusion walls, (2) one or several gas bubble(s) formed during thermal contraction, (3) some rare sulphide blebs (Fig. 2a), and (4) a pre-existing spinel crystal included during the inclusion formation (Fig. 2b). The pre-existing character of the spinel is shown by the fact that it never dissolves during experimental heating of the inclusions (Fig. 2b) and it occurs as an isolated phase inside the host olivine.

Table 1: Whole-rock major and trace element compositions

Lava:	HAOT	BA	BA	BA
Sample:	85-38	85-47	85-1a	95-15
Ref.:	1	2	1	1
Age:	>MH	SR	?	SR
SiO_2	49·14	53·12	51·52	50·93
TiO_2	0·87	0·7	0·56	0·66
Al_2O_3	16·95	17·32	15·55	15·54
FeO*	8·62	7·34	7·56	7·36
MnO	0·18	0·14	0·16	0·14
MgO	9·6	7·94	10·58	10·65
CaO	10·61	9·47	9·92	9·94
Na_2O	2·11	3·4	2·64	2·73
K_2O	0·3	0·43	0·38	0·76
P_2O_5	0·11	0·14	0·1	0·28
Total	98·49	100·00	98·97	98·99
$H_2O^{\dagger}$	>1		3·7	4·5
Cr	472	375	384	NA
Sr	204	354	291	682
Y	25	17	16	16
Zr	70	47	48	90
Nb	3·1	3·0	1·9	3·6
Ba	136	158	124	347
La	5·2	6·0	3·6	16·2

*All Fe reported as FeO.
†Primitive water content estimated from melt inclusions and high-pressure experimental studies and calculations based on equilibrium phase assemblage (for details, see Grove *et al.*, 2002).
HAOT, high-aluminium olivine tholeiite; BA, basaltic andesite; SR, Sargent Ridge age (<250 to >130 ka BP); MH, Misery Hill age (80–10 ka BP); (?), age unknown (Grove *et al.*, 2002). Reference 1, Grove *et al.* (2002); reference 2, Baker *et al.* (1994). Major elements normalized to 100% on an anhydrous basis.

HEATING TECHNIQUE

Correct selection (unaltered, prismatic crystals, containing well-preserved primary melt inclusions randomly distributed throughout the crystal and showing no cracks or links to the outside) is the mandatory first step to ensure the study of primary melt inclusions in equilibrium with the host olivine. The heating of the melt inclusions at 1 atm in a Vernadsky-type microscope heating stage allows direct visual observation of the melting phenomena during the heating run (Fig. 3). During the experiments, the oxygen fugacity was kept between 10^{-10} and 10^{-9} atm with He purified with Zr at 700°C, to avoid oxidation of the host mineral and to ensure an efficient quench. Each heating experiment lasted about 1 h, and the melt inclusions stayed at a temperature above 1100°C for less than 20 min (Fig. 3). The classical procedure corresponds to successive heating rates of 0·5°C/s for 20 min, 0·4°C/s for 20 min, 0·1°C/s until the last 'daughter' mineral has melted, and an additional 10 min at high temperature before quenching (Fig. 3). The persistence of the bubble inside the inclusions during the heating experiments (Fig. 3), even at temperatures as high as 1500°C, is likely to reflect the fact that melt inclusions do not behave as ideal isochoric systems

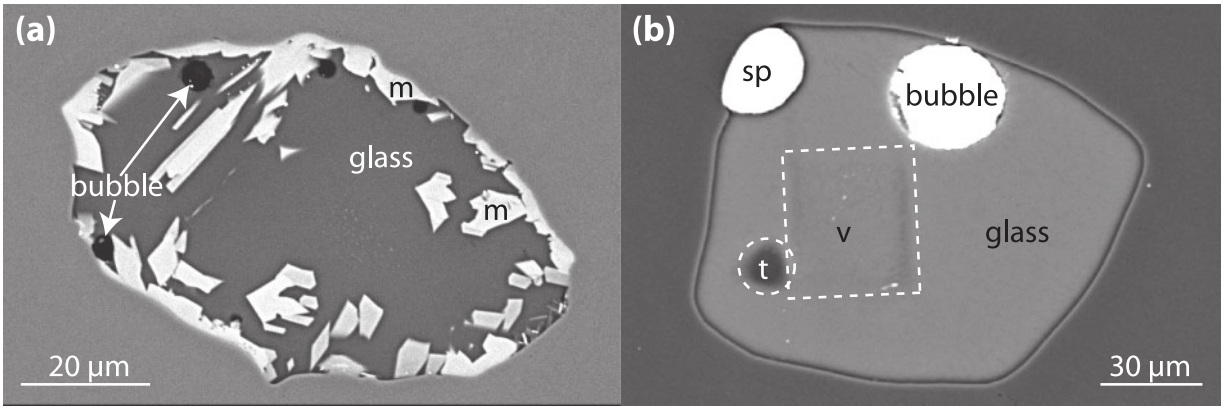

Fig. 2. Scanning electron microscope image (backscattered electron) of two Shasta olivine-hosted melt inclusions. (**a**) Partially crystallized melt inclusion before heating, with several bubbles and daughter minerals ('m', mostly clinopyroxene, orthopyroxene and olivine); (**b**) melt inclusion after heating and analysis: all the daughter minerals have melted to form a homogeneous glass, except for one pre-existing spinel ('sp'). Two analysis spots of the ion probe analyses are also visible ('t', trace element analysis; 'v', rastered area of the volatile element analysis).

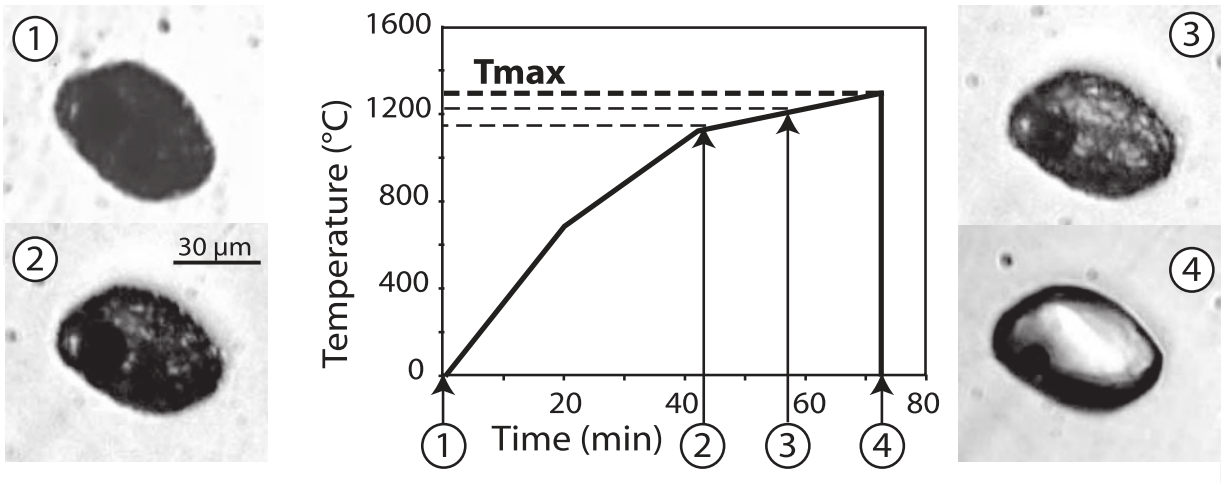

Fig. 3. Detail of the heating rates used during the heating procedure of the crystallized melt inclusions. Numbers 1–4 are transmitted light photomicrographs of a melt inclusion (2E1, from sample 85-38) during its heating: 1, the matrix of the melt inclusion is devitrified, hiding the daughter minerals; 2, lightening of the inclusion showing the beginning of the melting of the daughter minerals; 3, the daughter minerals are progressively melted; 4, all daughter minerals are melted, leaving only a bubble in a liquid matrix. T_{max} is the temperature of disappearance of the last daughter mineral.

during heating (Massare *et al.*, 2002; Schiano, 2003). Because of the inelastic behaviour of the olivine, the difference between the initial pressure of trapping and the internal pressure of the inclusions at high temperature (Schiano & Bourdon, 1999) prevents a complete homogenization. Alternatively, the presence of bubbles with potentially high CO_2 contents may also prevent the complete homogenization of the melt inclusions at 1 atm. As the melt inclusions have been heated only to the temperature of disappearance of the last daughter mineral (referred to as T_{max} subsequently), T_{max} represents a minimum estimate of their homogenization temperature (Fig. 3).

Several studies have suggested that diffusive loss of hydrogen and, possibly, hydroxyl can occur during 1 atm, long-term, homogenization procedures (Sobolev & Danyushevsky, 1994; Danyushevsky *et al.*, 2002; Hauri, 2002; Portnyagin *et al.*, 2007; Severs *et al.*, 2007). Molecular water may also be lost through dislocations that propagate in the host olivine (Massare *et al.*, 2002). To ensure that no volatile loss occurred during our heating procedure, heating-test runs were performed using a set of melt inclusions with known and clustered H_2O, CO_2, Cl, F and S compositions (Sommata melt inclusions from Vulcano, Italy; see Le Voyer, 2009, for more details about this test procedure). By comparing heated and non-heated samples, we found that our heating procedure does not result in significant loss of volatiles or in variations in the oxygen fugacity (determined from the sulphur speciation by

measuring the peak shift of the sulphur Kα radiation relative to a sulphide standard with the electron microprobe; Jugo *et al.*, 2005). Although hydrogen, for which diffusion is very rapid (Hauri, 2002), may certainly have diffused out of the inclusions during the heating, this did not seem to affect significantly the H_2O content or the oxygen fugacity of the heated inclusions.

ANALYTICAL METHODS

Major element compositions of olivine crystals and melt inclusions were obtained at the Laboratoire Magmas et Volcans (Clermont-Ferrand, France) using a Cameca SX 100 electron microprobe. We used a 15 kV accelerating voltage, an 8 nA current and a beam defocused to a size between 5 and 20 μm, depending on the diameter of the inclusion. No effect of alkali loss was observed on repeated analysis of the VG-A99 basaltic glass standard (Jarosewich *et al.*, 1979) under these conditions. Trace element analyses were carried out at the Woods Hole Oceanographic Institution (WHOI, MA, USA) using a Cameca IMS 3f ion probe. We used a 10 kV accelerating voltage of an O^- primary beam with a 6 nA intensity, a 4·5 kV secondary accelerating voltage, a −90 V offset, a mass resolving power of 300 and a projected beam size ranging from 10 to 20 μm. Each analysis consisted of four cycles starting from mass ^{7}Li, ^{11}B, ^{28}Si (reference mass), ^{52}Cr, ^{88}Sr, ^{89}Y, ^{91}Zr, ^{93}Nb, ^{137}Ba and ^{139}La. Each selected mass was counted for 20 s, except ^{28}Si (5 s). The data were corrected for oxide interferences (e.g. Fahey *et al.*, 1987). We used the basaltic reference glasses KL2-G and ML3B-G (Jochum *et al.*, 2006) to control and correct the instrumental drift and for the deconvolution procedure. Typical error on the samples (1σ error of mean; $\sigma/\sqrt{n}$, where n is the number of cycles) is less than 15% for all trace elements, except for B, Nb and La (<25%), which have low concentrations.

Volatile element analyses were carried out at WHOI using a CAMECA 1280 ion probe, following the procedure described by Rose-Koga *et al.* (2008) and Shimizu *et al.* (2009). As epoxy contains significant amounts of volatiles that would increase the background signal, the grains were removed from the epoxy mounts using a soldering iron, then pressed into a high-purity indium substrate, subjected to ultrasound in pure ethanol for 10 min followed by 10 min in distilled water, dried in a vacuum oven at ~120°C and ~10^{-3} torr for several hours and stored in a turbo-pump-based outgasser at ~10^{-7} torr for 4–12 h before gold coating. Prior to analysis, the sample was stored in the airlock of the instrument at ~5×10^{-9} torr before introducing it into the sample chamber at (2–4) × 10^{-9} torr. We used a Cs^+ primary ion beam with a current of ~1·5 nA, rastered over an area of 30 μm × 30 μm. The instrument was operated with the contrast aperture at 400 μm, the energy slit at 50 eV, the entrance slit at 80·9 μm and the exit slit at 176·8 μm with a mass resolving power of 5500, allowing the discrimination of interferences (^{34}S^{1}H over ^{35}Cl, ^{17}O over ^{16}O^{1}H, ^{29}Si^{1}H over ^{30}Si and ^{31}P^{1}H over ^{32}S). The field aperture was set to analyze the centre of a 15 μm × 15 μm area of a larger 30 μm × 30 μm sputter-cleaned area. After 3 min of pre-sputtering, we collected signals for ^{12}C (10 s), ^{16}O^{1}H (10 s), ^{19}F (5 s), ^{30}Si (5 s, reference mass), ^{32}S (5 s) and ^{35}Cl (5 s) (counting times in parenthesis), with a 2 s waiting time after each switch of the magnet. This cycle was repeated 10 times during one analysis. One measurement lasted 12 min per spot. The concentrations were determined using calibration curves obtained by measuring a set of natural basaltic glasses during the same session and under the same analytical conditions (D51-3, ALV519-4-1, 46D-2, 1649-3, D20-3, JD17H, 1654-3, 6001 and D52-5; Rose-Koga *et al.*, 2008) with a large range of concentrations of volatile elements overlapping most of our samples' concentrations (H_2O 0·05–2·49 wt%; CO_2 88–237 ppm, F 90–997 ppm, S 38–1640 ppm and Cl 45–2914 ppm). The maximum errors, taking into account the reproducibility over the 10 cycles of analyses and the errors on the regression of the calibration line, were less than 5% for H_2O and F, 15% for CO_2, and 10% for Cl and S, except for the melt inclusions from sample 85-38, which have low H_2O and Cl concentrations (errors of 25% and 50%, respectively).

Boron contents and boron isotope analyses were obtained at WHOI using a CAMECA 1280 ion probe following the procedure of Le Voyer *et al.* (2008). A primary beam of 13 nA of O_2^- was delivered onto the sample mounted in indium, with a nominal accelerating voltage of 12·5 kV. The secondary ion accelerating voltage was 10 kV, and the final impact energy was thus 22·5 kV. The mass resolution was set at 1974, high enough to separate isobaric interferences (the interference of mass ^{10}B^{1}H on mass ^{11}B is resolved with a resolution power higher than 1416 and the interference of mass ^{1}H^{9}Be on mass ^{10}B is resolved with a resolution power higher than 962). Köhler illumination was used. The size of the contrast aperture was 400 μm and that of the field aperture was 5000 μm. The energy window, which was initially centred on the optimized position for the ions, was opened to allow ions with a range of 50 eV into the mass spectrometer. No energy filtering was used. The samples were first pre-sputtered for 2 min to remove surface contaminants and then analyses were performed with a projected beam size between 20 and 30 μm. Each analysis was composed of 50 cycles: 9·7 (background, 3 s waiting time, 5 s analysis), ^{10}B (2 s waiting time, 30 s analysis), ^{11}B (2 s waiting time, 15 s analysis), $^{14}Si^{2+}$ (2 s waiting time, 3 s analysis) and lasted for about 55 min. Typical ^{10}B intensity measured on the samples was 1×10^3 c.p.s., down to rare minimum of 6×10^2 c.p.s. For each analysis we monitored the peak

intensity and the stability of the $^{11}B/^{10}B$ ratio. The instrumental mass fractionation, $\alpha_{instr} = \frac{(^{11}B/^{10}B)_{measured}}{(^{11}B/^{10}B)_{true}}$, was assessed by daily measurements of the GOR128-G and GOR132-G standards ($\delta^{11}B$ of $+13{\cdot}55 \pm 0{\cdot}11$‰ and $+7{\cdot}11 \pm 0{\cdot}48$‰; Jochum *et al.*, 2006). Boron isotopes in the samples are expressed in $\delta^{11}B$, where $\delta^{11}B = \left[\frac{(^{11}B/^{10}B)_{measured}/\alpha_{instr}}{(^{11}B/^{10}B)_{reference}} - 1\right] \times 1000$, relative to NIST SRM 951 ($^{11}B/^{10}B = 4{\cdot}04558 \pm 0{\cdot}00035$; Palmer *et al.*, 1987). We applied a signal drift correction scheme (data processing after acquisition with a Matlab program, doubly interpolated ratios variable in time) to both standard and sample analyses.

COMPOSITION OF MT. SHASTA PRIMITIVE MAGMAS

The olivine phenocrysts hosting the HAOT melt inclusions (sample 85-38) have Mg-number [$100 \times MgO/(MgO + FeO)$] of $86{\cdot}2 \pm 0{\cdot}2$% and CaO contents ranging from 0·24 to 0·27 wt% (Table 2). The olivine phenocrysts from the three BA samples (85-1a, 85-47 and 95-15 samples) have Mg-number ranging from 87·0 to 90·7% and CaO contents ranging from 0·14 to 0·21 wt% (Table 2). Some of the olivines show slight normal rim zonations. In both the HAOT and the BA samples, the Mg-number of most olivines are close to those required for olivine–liquid equilibrium (Mg-number from 86·5% for sample 85-38 to 90·5% for sample 95-15, taking the bulk lava content as representative for the liquid composition; Baker *et al.*, 1994). After heating, the compositions of some of the melt inclusions were corrected for post-entrapment olivine overgrowth by adding olivine until the inclusion and host mineral are in Mg/Fe equilibrium. The equilibrium value for the Mg/Fe exchange coefficient between olivine and liquid, K_D, has been estimated using the model proposed by Toplis (2005) and ranges from 0·28 to 0·33. In some cases, the melt inclusions were slightly overheated and required olivine subtraction (e.g. Sobolev & Chaussidon, 1996). The amount of added or subtracted olivine is lower than 12% (average of 5%). The corrected compositions of the Mt. Shasta melt inclusions are given in Table 2 for major elements and Table 3 for volatiles and trace elements.

Compositions of the HAOT melt inclusions

The HAOT melt inclusions (sample 85-38) are tholeiitic basalts (normative hypersthene 8 to 16%; Table 2) with clustered compositions. They have low SiO_2 (48·6–49·9 wt%) and low alkali contents (0·2 wt% K_2O; 2·4 wt% Na_2O). They are rich in MgO (8·4–10·1 wt%), FeO (7·8–9·4 wt%), Al_2O_3 (17·0–18·9 wt%), Nb (2–3 ppm) and Y (21–28 ppm; Tables 2 and 3; Figs 4 and 5). Their trace element patterns are very similar to normal mid-ocean ridge basalt (N-MORB) (Fig. 5b), showing only slight enrichment in B, Li, Sr and Ba and slight depletion in Y, Zr, Nb and La. They do not show the strong fractionation between large ion lithophile elements (LILE) and high field strength elements (HFSE) usually found in arc magmas. In terms of volatile element compositions, they are nearly anhydrous, with low and clustered contents of all volatile elements (average contents of 0·04 wt% H_2O, 380 ppm CO_2, 130 ppm F, 32 ppm Cl and 960 ppm S; Fig. 6; Table 3). Their volatile compositions are only slightly enriched in halogens compared with primitive Siqueiros MORB compositions (Saal *et al.*, 2002), which is unusual for typical arc magmas. They have lower volatile contents compared with the composition of olivine-hosted melt inclusions from other subduction zones (Fig. 6).

Composition of the BA melt inclusions

The BA melt inclusions (samples 85-1a, 85-47 and 95-15) have basalt to basaltic andesite compositions that are much more variable than the HAOT melt inclusions (SiO_2 46·5–51·6 wt% and MgO 8·0–10·6 wt%; Table 2; Fig. 4b). Their K_2O contents vary from 0·3 to 1·1 wt%, ranging from the tholeiite series to the calc-alkaline series (Fig. 4a). They also vary from hypersthene-normative compositions for the inclusions from samples 85-1a and 85-47 to nepheline-normative compositions for the inclusions from sample 95-15 (up to 6% of nepheline-normative; Table 2). They are enriched in B, Ba, Sr and La (up to 4·7 ppm, 485 ppm, 910 ppm and 19 ppm, respectively; Fig. 5) and depleted in Nb and Y (down to 0·2 and 9·6 ppm, respectively) compared with the HAOT melt inclusions (Table 3; Fig. 5). Their trace element patterns (Fig. 5) show the typical features of arc lavas: they are depleted in Nb and Ti (HFSE), enriched in Ba, K and Sr (LILE), and in La (light REE; LREE) relative to MORB. The melt inclusions from sample 95-15 are richer in K_2O, Na_2O, P_2O_5, Sr, Ba and La compared with the melt inclusions from samples 85-1a and 85-47. In contrast, the BA melt inclusions from samples 85-1a and 85-47 show an intermediate enrichment in fluid-mobile elements and in incompatible elements (Fig. 5). In terms of volatile element contents, the BA melt inclusions have compositions that range from nearly identical to the HAOT melt inclusions ('dry' end-member), to an enriched end-member with 2·6 wt% H_2O, 820 ppm CO_2, 1270 ppm Cl, 1220 ppm F and 6280 ppm S ('hydrous' end-member; Table 3; Fig. 6). Their CO_2, H_2O and Cl contents are included within the worldwide variation in composition of olivine-hosted melt inclusions from other arc settings (Fig. 6), having one of the lowest H_2O contents (Fig. 6a). In contrast, 95-15 BA melt inclusions have one of the highest F and S

Table 2: Major element compositions of the melt inclusions and their host olivines and T_{max} values

Sample:	85-38	85-38	85-38	85-38	85-38	85-38	85-38	85-38	85-38	85-38	85-38	85-38	85-38	85-38	85-38	85-1a	85-1a
Inclusion:	2E1a	2E1b	1H2b	1H2c	1H2d	1H2e	1D7	1H3	1J7a	1I2b	4A3	1I5a	2F5	2G8a	2G8b	1A4a	1J9
Olivine																	
SiO_2	40·77	40·77	40·60	40·60	40·60	40·60	40·19	39·99	40·21	40·30	40·43	40·87	40·37	40·44	40·44	40·50	40·75
FeO	13·00	13·00	13·13	13·13	13·13	13·13	13·17	13·10	13·28	13·13	13·15	13·03	13·10	13·08	13·08	10·67	8·74
MnO	0·21	0·21	0·18	0·18	0·18	0·18	0·20	0·19	0·20	0·20	0·17	0·17	0·19	0·16	0·16	0·17	0·15
MgO	45·51	45·51	46·26	46·26	46·26	46·26	46·85	46·43	45·96	45·94	45·45	46·21	46·75	46·78	46·78	48·38	47·16
CaO	0·25	0·25	0·26	0·26	0·26	0·26	0·24	0·26	0·25	0·25	0·27	0·25	0·26	0·26	0·26	0·20	0·18
NiO	0·05	0·05	0·04	0·04	0·04	0·04	0·06	0·06	0·01	0·05	0·07	0·04	0·02	0·06	0·06	0·22	0·28
Total	99·78	99·78	100·48	100·48	100·48	100·48	100·71	100·02	99·90	99·86	99·53	100·58	100·69	100·77	100·77	100·13	97·26
Mg-no.	86·18	86·18	86·27	86·27	86·27	86·27	86·38	86·33	86·05	86·18	86·04	86·34	86·42	86·44	86·44	88·99	90·58
Inclusion																	
T_{max}	1345	1345	1276	1276	1276	1276	1342	1324	1349	1339	1438	1345	1321	1350	1350	—	1316
SiO_2	49·19	48·57	49·11	49·36	48·94	48·74	49·23	49·31	48·84	49·89	48·91	49·57	48·59	49·37	48·65	50·77	50·05
TiO_2	0·92	0·82	0·88	0·93	0·87	0·85	0·95	0·94	0·86	0·91	0·93	0·97	0·86	0·85	0·83	0·61	0·50
Al_2O_3	18·64	17·99	18·66	18·89	18·02	18·07	18·12	18·67	18·51	18·80	18·47	18·78	18·20	17·99	18·03	17·95	16·70
FeO*	8·27	8·89	8·66	8·45	9·11	9·37	8·69	8·19	8·54	8·17	8·31	7·82	9·42	8·87	9·11	6·39	6·10
MnO	0·12	0·11	0·15	0·22	0·25	0·22	0·21	0·23	0·17	0·09	0·14	0·10	0·14	0·29	0·20	0·12	0·18
MgO	8·82	9·38	8·82	8·41	9·45	9·61	9·09	8·56	8·62	8·60	8·97	8·54	10·06	9·58	10·03	8·36	9·37
CaO	11·00	10·82	10·91	11·14	10·82	10·94	11·04	11·33	11·17	10·96	10·86	11·39	10·56	10·64	10·63	11·16	10·19
Na_2O	2·33	2·33	2·50	2·37	2·19	2·24	2·54	2·53	2·49	2·53	2·39	2·70	2·29	2·17	2·17	2·69	2·29
K_2O	0·18	0·17	0·19	0·19	0·17	0·17	0·21	0·20	0·20	0·21	0·19	0·19	0·17	0·18	0·18	0·32	0·60
P_2O_5	0·07	0·08	0·06	0·12	0·08	0·03	0·08	0·06	0·08	0·08	0·10	0·10	0·06	0·08	0·13	0·06	0·07
Total	99·55	99·15	99·96	100·08	99·90	100·24	100·15	100·01	99·47	100·23	99·27	100·16	100·34	100·04	99·96	98·43	96·04
ne	0·00	0·00	0·00	0·00	0·00	0·00	0·00	0·00	0·00	0·00	0·00	0·00	0·00	0·00	0·00	0·00	0·00
hy	12·36	11·84	8·36	12·16	13·06	9·17	8·81	9·32	9·19	11·74	12·86	8·29	8·89	15·69	12·07	15·43	21·53

Sample:	85-1a	85-1a	85-1a	85-1a	85-1a	85-1a	85-47	85-47	85-47	85-47	95-15	95-15	95-15	95-15	95-15	95-15	95-15
Inclusion:	3A6	3G6	3C4	3J6a	3J6b	1E5	1K5a	1K5c	1A1	1I5	2A3b	2D3a	2D3b	2I5	1L8a	2I8	2I2
Olivine																	
SiO_2	41·63	41·32	41·32	41·32	41·32	41·32	40·78	40·78	41·25	41·33	41·47	41·56	41·56	41·56	40·65	40·64	40·58
FeO	10·14	10·36	10·17	9·69	9·69	11·50	9·61	9·61	10·13	9·85	8·96	10·15	10·15	10·59	11·59	9·79	10·71
MnO	0·16	0·18	0·14	0·15	0·15	0·13	0·13	0·13	0·14	0·15	0·15	0·20	0·20	0·14	0·21	0·17	0·14
MgO	48·07	48·30	48·51	48·31	48·31	46·88	48·43	48·43	48·13	47·67	49·13	48·17	48·17	47·28	48·08	49·25	48·79
CaO	0·18	0·19	0·21	0·18	0·18	0·17	0·17	0·17	0·14	0·16	0·17	0·16	0·16	0·14	0·20	0·19	0·14
NiO	0·28	0·27	0·30	0·31	0·31	0·27	0·40	0·40	0·37	0·38	0·42	0·18	0·18	0·30	0·23	0·32	0·26
Total	100·47	100·61	100·63	99·95	99·95	100·25	99·51	99·51	100·17	99·53	100·30	100·41	100·41	100·01	100·96	100·35	100·62
Mg-no.	89·41	89·26	89·48	89·88	89·88	87·90	89·98	89·98	89·44	89·61	90·72	89·43	89·43	88·84	88·09	89·97	89·04
Inclusion																	
T_{max}	1239	1268	1211	1261	1261	1209	1283	1283	1307	1299	1296	1225	1225	1227	1253	1171	1188
SiO_2	50·89	49·86	49·87	49·83	49·76	51·58	49·25	50·25	50·13	48·65	47·64	48·15	51·16	46·53	48·14	47·70	46·57
TiO2	0·52	0·50	0·47	0·51	0·53	0·56	0·57	0·49	0·62	0·64	0·78	0·73	0·67	0·85	0·80	0·75	0·77
Al_2O_3	17·58	18·07	17·39	17·99	18·33	17·63	16·95	15·95	19·20	19·06	16·99	16·72	15·67	17·67	18·67	16·91	15·86
FeO*	6·60	6·34	6·26	6·04	6·30	7·24	7·37	7·11	6·70	7·25	6·88	6·87	6·62	6·86	7·32	6·49	7·33
MnO	0·10	0·15	0·06	0·04	0·03	0·17	0·14	0·16	0·09	0·16	0·14	0·12	0·20	0·25	0·22	0·17	0·14
MgO	8·61	8·61	8·63	8·61	8·78	8·40	10·55	10·28	8·75	9·57	10·43	8·80	8·76	8·24	8·02	8·81	9·13
CaO	10·80	11·35	11·16	11·32	11·39	9·43	10·17	10·03	10·61	10·95	11·06	11·16	10·45	11·67	12·08	11·28	10·96
Na_2O	2·53	2·53	2·58	2·61	2·58	2·65	2·63	2·41	3·09	3·04	2·70	2·80	2·66	3·23	3·26	2·87	2·96
K_2O	0·30	0·30	0·28	0·31	0·32	0·44	0·29	0·26	0·37	0·35	0·99	0·78	0·79	1·11	0·89	0·85	0·98
P_2O_5	0·06	0·09	0·09	0·08	0·14	0·08	0·08	0·12	0·08	0·07	0·45	0·29	0·25	0·40	0·31	0·35	0·37
Total	97·99	97·80	96·80	97·32	98·17	98·18	98·00	97·07	99·64	99·71	98·05	96·42	97·24	96·81	99·70	96·17	95·08
ne	0·00	0·00	0·00	0·00	0·00	0·00	0·00	0·00	0·00	1·04	0·04	1·13	0·00	3·57	6·41	0·00	0·05
hy	17·96	15·40	16·92	14·62	8·98	27·62	12·01	23·28	5·79	0·00	0·00	0·00	15·30	0·00	0·00	3·27	0·00

(continued)

Table 2: Continued

Sample:	95-15	95-15	95-15	95-15	95-15	95-15	95-15	95-15	95-15	95-15	95-15	95-15	95-15	95-15	95-15	95-15
Inclusion:	2J5	2H7	8A	1Aa	2A	5Aa	5Ab	14B	15B	16Ba	16Bb	20B	12Bb	5B	4Ba	3A
Olivine																
SiO_2	41·58	41·60	40·71	40·50	40·87	40·33	40·33	40·38	40·90	40·59	40·59	40·58	40·13	40·33	40·14	40·59
FeO	9·91	10·48	9·39	10·16	10·03	9·85	9·85	10·37	10·36	9·43	9·43	9·87	11·68	9·78	12·43	9·52
MnO	0·15	0·14	0·13	0·15	0·14	0·17	0·17	0·15	0·19	0·11	0·11	0·15	0·18	0·17	0·19	0·17
MgO	47·36	47·72	48·84	48·60	48·62	48·81	48·81	47·78	48·15	48·74	48·74	48·51	47·53	48·69	46·72	49·06
CaO	0·15		0·17	0·19	0·15	0·17	0·17	0·17	0·16	0·19	0·19	0·17	0·17	0·17	0·18	0·18
NiO	0·33	0·37	0·33	0·26	0·35	0·30	0·30	0·28	0·27	0·32	0·32	0·30	0·17	0·34	0·15	0·32
Total	99·49	100·31	99·56	99·86	100·16	99·64	99·64	99·13	100·02	99·38	99·38	99·58	99·85	99·49	99·81	99·85
Mg-no.	89·49	89·03	90·27	89·50	89·63	89·83	89·83	89·15	89·23	90·21	90·21	89·76	87·88	89·87	87·01	90·18
Inclusion																
T_{max}	1208	1245	1230	1230	1230	1230	1230	1230	1230	1230	1230	1230	1230	1230	1230	1230
SiO_2	50·88	47·03	47·18	47·69	47·69	48·19	47·76	48·02	48·72	47·48	47·30	47·80	48·40	46·94	47·79	50·95
TiO_2	0·58	0·52	0·78	0·71	0·78	0·78	0·76	0·77	0·77	0·74	0·72	0·69	0·72	0·82	0·75	0·62
Al_2O_3	17·30	17·17	17·57	17·06	17·32	17·17	17·86	17·20	17·97	16·81	17·64	17·04	15·67	17·37	16·76	15·90
FeO*	6·54	7·91	6·37	7·10	6·99	6·87	6·62	7·12	6·67	6·83	6·56	6·55	7·64	6·79	8·71	6·15
MnO	0·09	0·15	0·15	0·15	0·11	0·06	0·11	0·18	0·09	0·08	0·18	0·08	0·08	0·08	0·07	0·10
MgO	8·68	9·80	8·59	8·90	8·86	8·87	8·61	8·69	8·11	9·06	8·84	8·42	8·42	8·85	8·81	8·64
CaO	9·73	12·39	11·90	11·77	11·43	11·69	12·14	11·20	11·57	11·41	11·93	11·71	10·61	11·62	10·62	10·98
Na_2O	2·93	2·64	3·13	3·02	3·04	3·05	3·06	3·05	3·13	2·84	3·02	2·92	2·73	3·16	2·89	3·10
K_2O	0·70	1·05	0·92	0·85	0·83	0·85	0·82	0·86	0·91	0·75	0·86	0·77	0·75	0·88	0·84	0·84
P_2O_5	0·11	—	0·30	0·34	0·33	0·32	0·37	0·33	0·34	0·28	0·27	0·28	0·27	0·32	0·28	0·17
Total	97·54	98·68	96·88	97·58	97·39	97·84	98·12	97·42	98·29	96·29	97·32	96·26	95·27	96·82	97·51	97·45
ne	0·00	5·68	6·15	4·72	4·12	4·08	5·12	3·40	3·46	2·81	5·62	2·97	0·00	6·19	2·26	0·00
hy	16·89	0·00	0·00	0·00	0·00	0·00	0·00	0·00	0·00	0·00	0·00	0·00	3·29	0·00	0·00	2·47

*Total iron given as FeO.
The melt inclusion compositions have been corrected to be in Fe–Mg equilibrium with their host olivine. Major elements are given in wt%. T_{max} is the temperature of disappearance of the last daughter mineral during heating. Mg-number is the molar ratio $Mg/(Mg + Fe) \times 100$ in the host olivine. a, b and c at the end of the inclusion names distinguish several inclusions from the same olivine grain. ne and hy are CIPW nepheline and hypersthene normative content, respectively, calculated from Cross *et al.* (1903), assuming all Fe as FeO.

concentrations for a given Cl concentration compared with melt inclusions from arc settings (Fig. 6b and c). The volatile contents of the BA melt inclusions do not seem to correlate with refractory trace elements of similar incompatibility. The estimated H_2O–CO_2 saturation pressures of the BA melt inclusions range from 0·2 to 2·0 kbar (Table 3; Fig. 6a). This pressure range represents a minimum estimate of the entrapment pressure of the inclusions, as CO_2 loss into shrinkage bubbles, as a result of the post-entrapment thermal contraction of the melt, and inclusion crystallization are not taken into account. To our knowledge, there are no seismic data to constrain the depth of the magma chamber beneath Mount Shasta. Based on geochemical and petrological data, Grove *et al.* (2005) suggested that olivine fractionated in two magma reservoirs at crustal depths (7–10 km and 15–25 km, corresponding to 2–8 kbar); that is, at higher pressures than the estimated H_2O–CO_2 saturation pressures.

Boron isotope measurements have been performed on two 85-47 melt inclusions, two 85-1a melt inclusions and four 95-15 melt inclusions (Table 4). The $\delta^{11}B$ from the 85-1a and 85-47 melt inclusions ranges between $-4{\cdot}9 \pm 1{\cdot}1‰$ and $+4{\cdot}4 \pm 1{\cdot}1‰$, whereas the 95-15 melt inclusions have lower $\delta^{11}B$ values ($-10{\cdot}2 \pm 1{\cdot}3‰$ to $-3{\cdot}2 \pm 0{\cdot}9‰$), within the range of previously reported $\delta^{11}B$ variations for 95-15 melt inclusions ($-21{\cdot}3 \pm 2{\cdot}5‰$ to $-0{\cdot}9 \pm 2{\cdot}7‰$; Rose *et al.*, 2001). The $\delta^{11}B$ variations in the BA melt inclusions are larger than the variations observed for the Cascade whole-rocks ($-9{\cdot}1 \pm 0{\cdot}5‰$ to $-0{\cdot}4 \pm 0{\cdot}5‰$, Leeman *et al.*, 2004), including positive $\delta^{11}B$ values that have not been reported for whole-rock lavas.

Table 3: Representative trace and volatile element compositions of melt inclusions

Sample:	85-38	85-38	85-38	85-38	85-38	85-38	85-38	85-38	85-1a	85-1a	85-1a	85-1a	85-1a	85-1a	85-1a	85-47	85-47
Inclusion:	2E1a	2E1b	1D7	1H3	1J7a	1I2b	4A3	1I5a	1A4a	1J9	3G6	3C4	3J6a	3J6b	1E5	1K5a	1K5c
H_2O		0·03	0·04	0·04	0·04		0·05		0·55	0·03	2·00	2·46	2·15		1·88	1·65	2·16
CO_2		—	—	374	472		300		111	317	492	500	738		169	—	—
F		127	148	123	139		134		217	16	135	138	159		159	171	169
S		1156	941	874	917		915		—	—	937	1075	878		769	807	744
Cl		29	33	31	33		32		619	450	633	642	655		508	618	624
P_{sat}				0·8	1·0		0·6		0·3	0·7	1·4	1·7	2·0		0·7		
Li	6·2		5·6	5·6	5·9	7·0	6·5	6·5	6·3	3·9	4·8	6·0	5·1	3·6	4·1	3·6	7·8
B	0·5		0·5	0·6	b.d.l.	1·3	1·8	2·8	3·5	3·0	b.d.l.	2·1	4·7	4·1	2·6	2·5	3·6
Sr	186		177	194	201	185	191	153	278	166	315	235	315	295	275	259	211
Y	28		26	28	27	21	28	24	14	10	16	12	14	13	12	11	20
Zr	80		63	73	74	61	59	49	47	27	46	27	46	43	37	39	59
Nb	b.d.l.		2·5	3·0	2·7	b.d.l.	2·4	2·3	0·2	0·6	1·5	1·2	0·9	0·7	0·7	1·4	1·4
Ba	85		100	97	101	85	99	84	145	53	90	75	90	90	124	92	79
La	1·9		2·3	4·6	3·8	2·7	4·3	3·2	2·4	2·6	5·6	2·5	3·3	2·3	3·2	3·0	2·9

Sample:	85-47	85-47	95-15	95-15	95-15	95-15	95-15	95-15	95-15	95-15	95-15	95-15	95-15	95-15	95-15	95-15
Inclusion:	1A1	1I5	2I5	2I8	2I2	2J5	1	3	4	8	9	10	11	12	16	17
H_2O	0·60	0·10	2·02	1·96	2·45	1·82	0·93	1·09	1·41	1·19	1·14	1·96	2·13	2·60	1·27	1·25
CO_2	533	111	714	381	658	251	483	372	825	222	503	570	570	141	459	153
F	171	170	1217	950	1171	454	833	682	993	850	875	833	800	821	934	821
S	517	512	3681	3398	4618	731	2486	4094	1775	1929	6285	2576	2313	2320	1903	1666
Cl	511	597	1268	1025	1143	849	806	722	897	955	858	968	942	923	1039	891
P_{sat}	1·2	0·2	1·2	0·9	1·4	0·9	1·1	0·9	1·9	0·6	1·2	1·6	1·7	1·0	1·1	0·5
Li	4·1	—	8·5	3·7	4·9	6·4	2·5	2·4	2·2	5·0	4·8	5·1	5·0	5·1	4·7	5·4
B	3·2	0·2	2·8	2·8	2·6	—	1·8	1·8	2·0	2·7	2·3	2·3	2·5	2·6	2·5	2·5
Sr	291	304	911	712	835	476	830	628	833	767	789	727	719	669	851	766
Y	11	12	14	14	13	12	18	13	17	17	17	19	19	16	18	17
Zr	45	52	—	84	87	72	101	59	95	101	97	98	102	94	108	98
Nb	1·1	2·4	3·3	2·6	3·7	1·8	4·8	2·9	4·4	4·4	4·4	4·5	5·1	3·9	4·4	4·3
Ba	125	110	485	402	446	253	448	312	433	411	427	416	395	369	451	408
La	3·8	1·7	19·1	16·2	15·1	9·9										

H_2O concentrations are given in wt%. CO_2, Cl, F, S, and trace element concentrations are given in ppm. P_{sat} is H_2O–CO_2 saturation pressure, in kbar, calculated using VolatilCalc (Newman & Lowenstern, 2002) and average values of 49 wt% SiO_2 and 1230°C. b.d.l., below detection limit.

Do the volatile contents of the Mt. Shasta melt inclusions represent the composition of the primary melt?

Melt inclusions trapped in early formed minerals are potentially undegassed and therefore hold clues to the primitive volatile composition of the magmas (e.g. Métrich & Wallace, 2008). However, even if there has not been any volatile loss during our heating procedure, it does not mean that the measured volatile contents are the primary volatile contents. Natural processes may have altered the primary volatile content of the Shasta melt inclusions: (1) early degassing of the magma prior to the entrapment of the melt inclusions (e.g. Métrich & Wallace, 2008); (2) diffusion of hydrogen during natural cooling (Danyushevsky *et al.*, 2002); (3) crystallization of sulphides in the melt inclusions. As a consequence of the low solubility of CO_2 in basaltic magmas, most of them are saturated with CO_2-rich vapour at mantle pressures

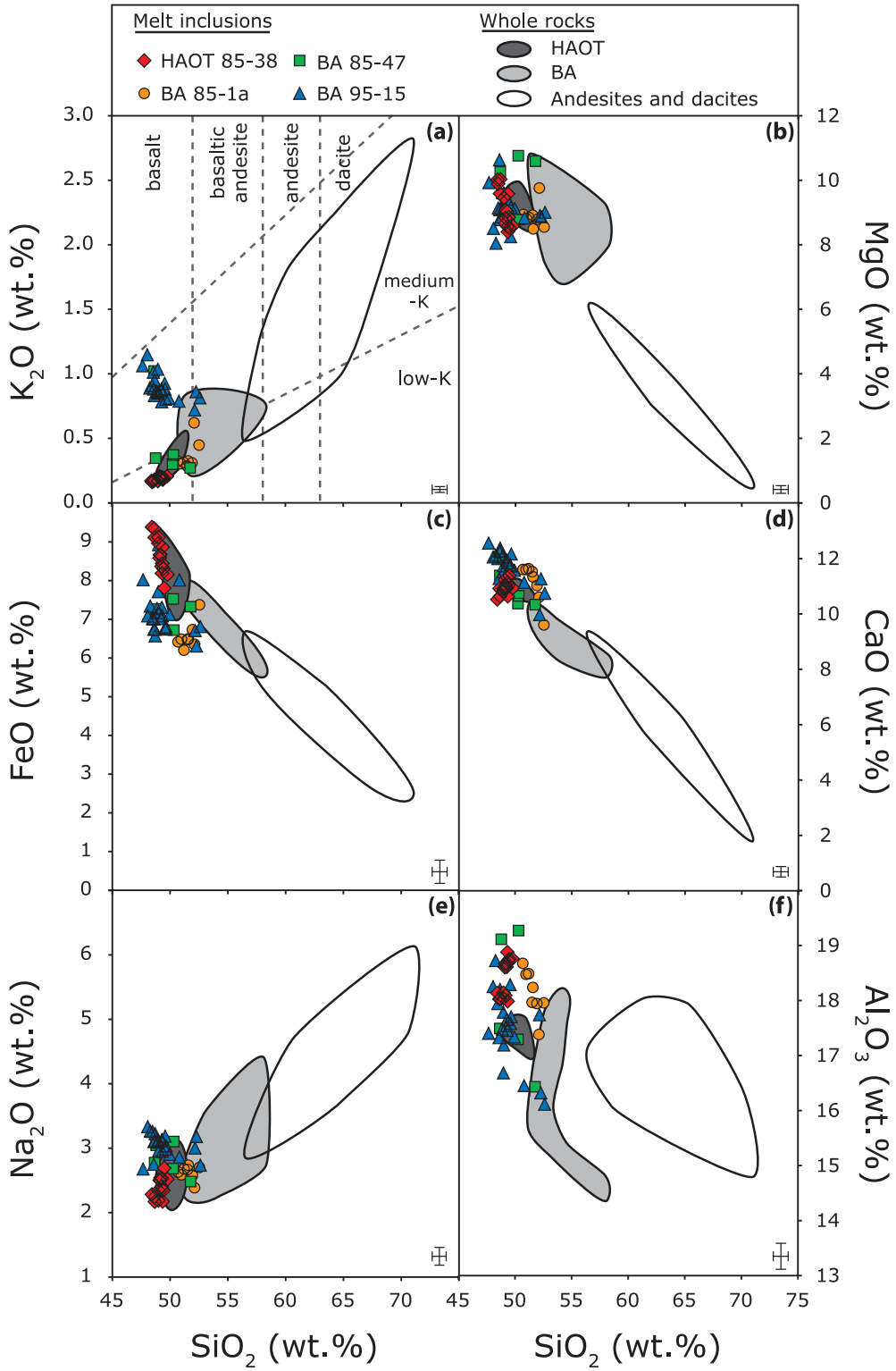

Fig. 4. SiO_2 variations as a function of (**a**) K_2O, (**b**) MgO, (**c**) FeO, (**d**) CaO, (**e**) Na_2O and (**f**) Al_2O_3 in the melt inclusions trapped in olivine phenocrysts from Mt. Shasta basic lavas. Classification boundaries in (a) are from Peccerillo & Taylor (1976). Also shown for comparison are the compositions of the whole-rock lavas from Mt. Shasta (black, grey and white fields; Baker *et al.*, 1994; Grove *et al.*, 2002, 2005). All major element compositions have been recalculated to 100% on a volatile-free basis. Error bars (±2σ) represent average analytical errors on the melt inclusion compositions.

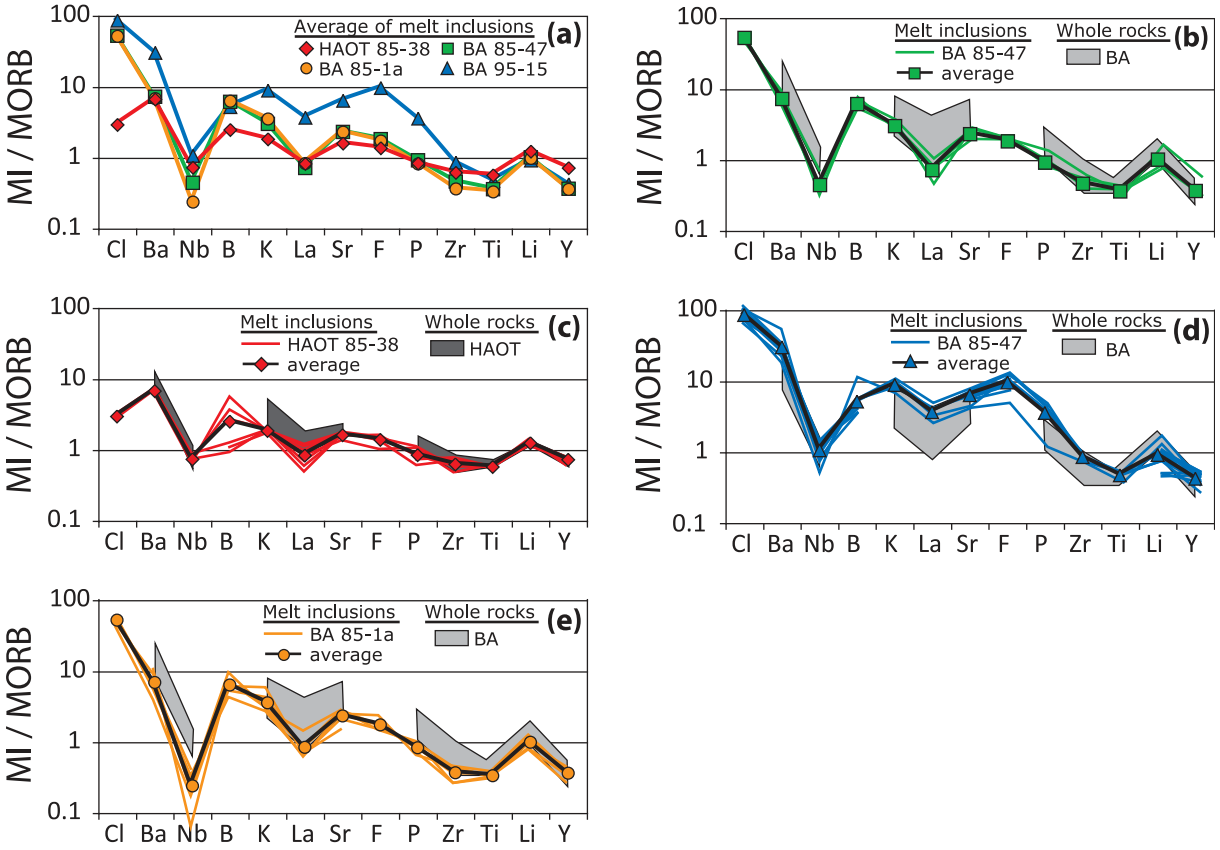

Fig. 5. (**a–e**) Trace element compositions of Shasta melt inclusions normalized to the average N-MORB composition (Hofmann, 1988; except for Cl and F, Saal *et al.*, 2002; B, Chaussidon & Marty, 1995; Li, Elliott *et al.*, 2004). Also shown for comparison in (b–e) are the whole-rock compositions of lavas from Mt. Shasta (grey fields; Baker *et al.*, 1994; Grove *et al.*, 2002, 2005). Although the trace element patterns of the HAOT melt inclusions are relatively flat compared with MORB, they still have characteristics of arc lavas, with, for example, a negative Nb anomaly. The BA melt inclusion patterns show more pronounced features typical of arc lavas: they are depleted in Nb and Ti (HFSE), enriched in Ba, K and Sr (LILE), and in La (LREE) relative to MORB.

(Métrich & Wallace, 2008). As the Mt. Shasta melt inclusions have been trapped at relatively shallow depths (0·2–2·0 kbar; Table 3; Fig. 6a), their parental melts may have already lost part of their CO_2 content. Second, even though there has not been any significant water loss during experimental heating, we cannot exclude hydrogen diffusion out of the olivine during natural cooling of the samples. In the case of the BA melt inclusions, their H_2O contents (0·1–2·6 wt%) are lower than the estimated H_2O contents of the BA lavas (3–5 wt% H_2O; Baker *et al.*, 1994; Grove *et al.*, 2002). In the case of the HAOT melt inclusions, although their mobile trace elements and their Cl (29–33 ppm) contents are higher than those of primitive MORB (Hofmann, 1989; 1–21 ppm Cl; Saal *et al.*, 2002), they are depleted in H_2O (0·03–0·05 wt%) compared with primitive MORB (0·04–0·12 wt%; Saal *et al.*, 2002; Fig. 6a). They may have lost part of their original H_2O by diffusion through the olivine host during slow cooling of the lava flows as a result of their high eruptive temperatures. Third, if the melt is supersaturated in S, then the formation of sulphides in some of the HAOT and BA melt inclusions may have lowered their S contents. The S content of the 95-15 melt inclusions shows a strong decrease with respect to Cl (Fig. 6c). This decrease is related to either degassing or removal by sulphide upon crystallization and cooling of the entrapped melts. However, two melt inclusions from sample 95-15 (inclusions 9 and 212, with 6285 and 4618 ppm S, respectively; Table 3; Fig. 6c) show extremely high S contents and therefore may have retained their initial S contents. With this range of observations, we suggest that the H_2O, CO_2 and S pre-eruptive contents of the Mt. Shasta melt inclusions are mostly underestimations of the primitive contents of the magma. This minimum estimation is nevertheless still a useful parameter, as it provides more constraints on the volatile composition of the primary magma than the composition of the degassed matrix glass or the bulk lava. In contrast,

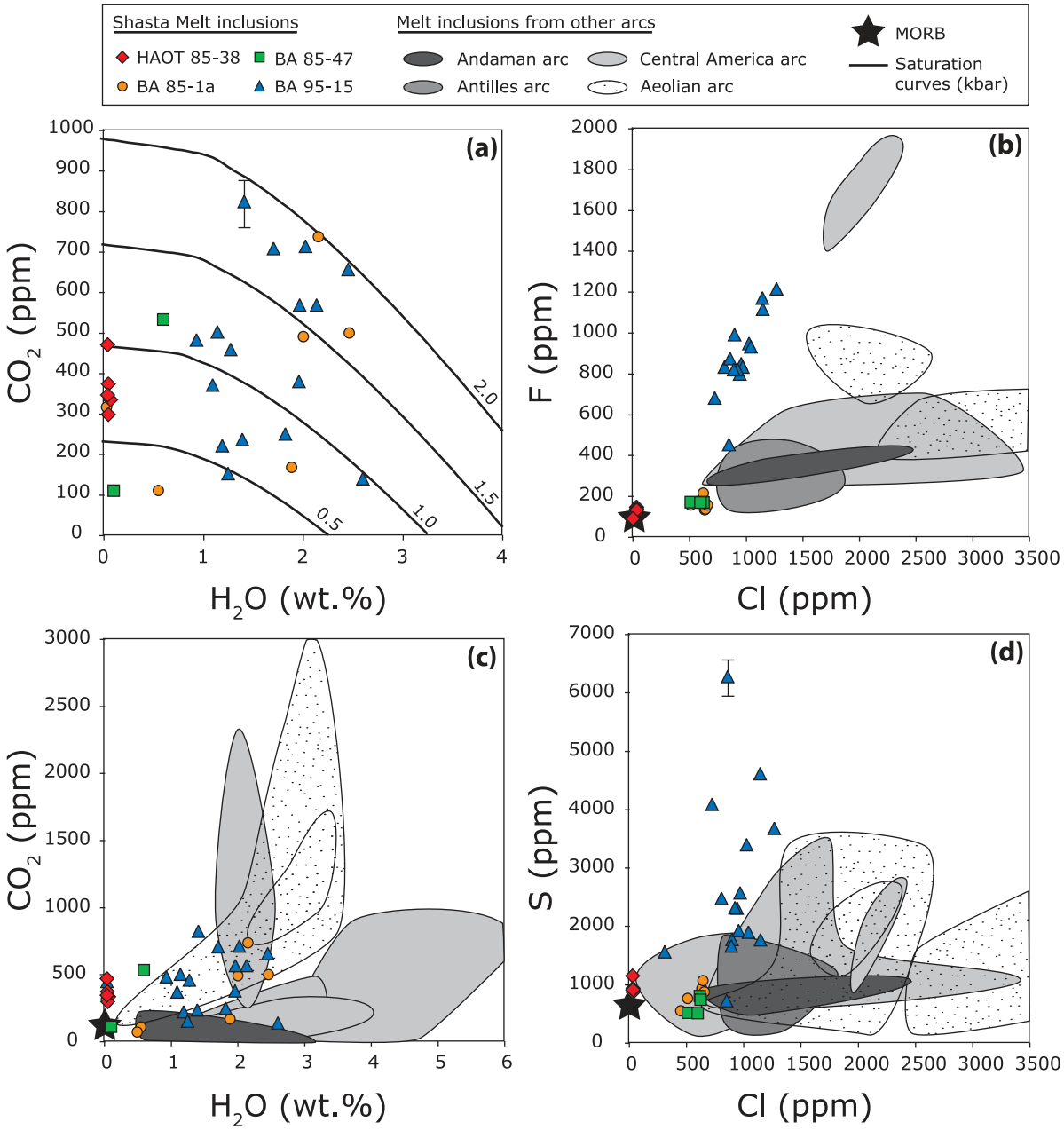

Fig. 6. Volatile concentrations in Shasta melt inclusions: (**a, c**) H_2O vs CO_2; (**b**) Cl vs F; (**d**) Cl vs S. The volatile compositions of the HAOT melt inclusions are clustered and close to the primitive MORB composition. In contrast, the BA melt inclusions range in composition from the HAOT melt inclusions to a hydrous end-member enriched in volatile elements. Primitive MORB compositions (black star; Saal *et al.*, 2002), as well as the compositions of olivine-hosted melt inclusions from other arc lavas (grey shaded and stippled fields, compiled from the GEOROC database; Andaman arc: Luhr *et al.*, 2006; Antilles arc: Bouvier *et al.*, 2008; Central America arc: Roggensack *et al.*, 1997; Walker *et al.*, 2003; Wade *et al.*, 2006; Benjamin *et al.*, 2007; Aeolian arc: Métrich *et al.*, 1993, 2001*l*; Gioncada *et al.*, 1998; Bertagnini *et al.*, 2003; Spilliaert *et al.*, 2006) are shown for comparison. In (a), H_2O–CO_2 saturation curves have been calculated using VolatileCalc (Newman & Lowenstern, 2002) with average values of 49 wt% SiO_2 and 1230°C. Error bars ($\pm 1\sigma$) represent maximum analytical errors on one of the most volatile-rich melt inclusions. If not shown, errors are smaller than the symbols.

Cl and F do not show any sign of degassing. This is consistent with (1) the highest solubility of these volatile species in mafic melts compared with CO_2 or H_2O (Webster, 2004), and (2) their late degassing during magma ascent (Spilliaert *et al.*, 2006). Therefore, we consider in the following discussion that the F and Cl contents of the Mt. Shasta melt inclusions represent the contents of the primary magma prior to any degassing processes, but that

Table 4: B contents and B isotopic compositions of the BA melt inclusions

Sample:	85-1a	85-1a	85-47	85-47	95-15	95-15	95-15	95-15
Inclusion:	3C4	1E5	1K5a	1I5	2I5	2I8	2I2	2H7
B	2·0	1·6	2·0	2·5	2·4	2·1	2·3	0·10
$\delta^{11}B$	+4·2	−4·9	−4·1	+4·4	−10·2	−9·8	−3·2	−5·2
σ_m	1·0	1·1	1·4	1·1	1·3	1·1	0·9	0·6

$\delta^{11}B$ is given in ‰. σ_m is 1σ error of mean ($\sigma/\sqrt{n}$, where n is the number of analytical cycles).

the H_2O, CO_2 and S are minimum estimations of its primary volatile content.

DISCUSSION

Iron loss

Several studies have demonstrated that Fe–Mg post-entrapment re-equilibration between the inclusion and the host olivine can lead to modification of the FeO content of the inclusion (e.g. Danyushevsky *et al.*, 2000, 2002). The main evidence commonly used to detect Fe loss in melt inclusions is the lower FeO contents of the melt inclusions compared with the whole-rock compositions, associated with a high Fe–Mg partition coefficient K_D between the melt inclusions and the host olivine (Danyushevsky *et al.*, 2000). In the case of the HAOT melt inclusions, their FeO contents (7·8–9·4 wt%) are either within the range of the FeO content of the HAOT lavas (6·5–8·5 wt%; Baker *et al.*, 1994; Grove *et al.*, 2002) or slightly higher. Therefore they do not seem to have suffered from Fe loss. However, some of the BA melt inclusions show FeO contents (down to 6·0 wt%) lower than those of the BA lavas (5·6–7·9 wt%; Baker *et al.*, 1994; Grove *et al.*, 2002) associated with high K_D values (up to 0·46). Correction for Fe loss (Danyushevsky *et al.*, 2000) requires an arbitrary estimation of the initial FeO content in the inclusion, generally by using the FeO content of the host lava. Here the large variation in FeO content of the BA lavas complicates the choice of the initial FeO value. Moreover, the case of the HAOT melt inclusions demonstrates that the initial FeO value may be higher that the FeO content of the host lavas. To assess the information given by the major-element compositions of the melt inclusions without correcting them for post-entrapment re-equilibration, we have recalculated the melt inclusion compositions into equivalent $CaO–MgO–Al_2O_3–SiO_2$ (CMAS) and then projected from olivine onto the diopside–nepheline–quartz face of the basalt tetrahedron (Fig. 7; Falloon & Green, 1988). Such a projection circumvents the possible effect of (1) host olivine crystallization on the walls of the melt inclusions, (2) overheating (and thus melting) of the host olivine and (3) re-equilibration between the host olivine and the melt inclusions (Laubier *et al.*, 2007). It should be noted that incompatible trace elements remain relatively unaffected by olivine-inclusion re-equilibration (Cottrell *et al.*, 2002); therefore they can be used, combined with volatile elements, to model the source of the Shasta melt inclusions.

Consistency of the melt inclusion results with lava compositions and petrological models

Case of the HAOT melt inclusions

The HAOT melt inclusion compositions were compared with experimental melts of lherzolite obtained at 10 and 15 kbar in a CMAS model system (Fig. 7a). The HAOT melt inclusions (diamonds in Fig. 7a) plot in the tholeiite field, close to the HAOT lavas (Baker *et al.*, 1994; Grove *et al.*, 2002). Their compositions are consistent with the compositional range of experimental dry lherzolite melts (hatched area in Fig. 7a; Hirose & Kushiro, 1993; Baker & Stolper, 1994; Baker *et al.*, 1995; Kushiro, 1996; Laporte *et al.*, 2004). Either a variation in composition (i.e. chemical heterogeneity of the source) and/or a variation of melting degree (black arrow in Fig. 7a) may cause the small variations observed in the major element compositions of the HAOT melt inclusions. Based on melting experiments and previous studies of HAOT lavas (Baker *et al.*, 1994; Grove *et al.*, 2002), we simply propose that the HAOT melt inclusions derive from the melting of a relatively dry lherzolitic mantle source. To account for the trace element patterns of the HAOT melt inclusions (in particular the slight enrichment in B and Ba compared with MORB, Fig. 5b), this lherzolitic mantle may have previously been slightly enriched by a slab-derived component. This source is similar to that proposed for the HAOT whole-rocks by Baker *et al.* (1994). This interpretation is supported by the close match in major and trace element compositions between the HAOT lavas and the HAOT melt inclusions (Figs 4 and 5) and by the nearly anhydrous, low volatile contents of the HAOT melt inclusions (Fig. 6). Their Nb/Y, H_2O/Y, Cl/Y ratios (respective averages of 0·1, 20 and 1·3) are consistent with those of a depleted MORB mantle source (~0·1, <100 and <2, respectively; Métrich & Wallace, 2008). Moreover, the temperatures of disappearance of the last daughter minerals during the heating of the HAOT melt inclusions (average of 1320°C for the melt inclusions from sample 85-38) are consistent with estimates of the temperature of last equilibration with the upper mantle inferred from HAOT lavas compositions (1300°C, Bartels *et al.*, 1991; Baker *et al.*, 1994; Elkins & Grove, 2001). Therefore, the information given by the melt inclusions is consistent with previous studies of the

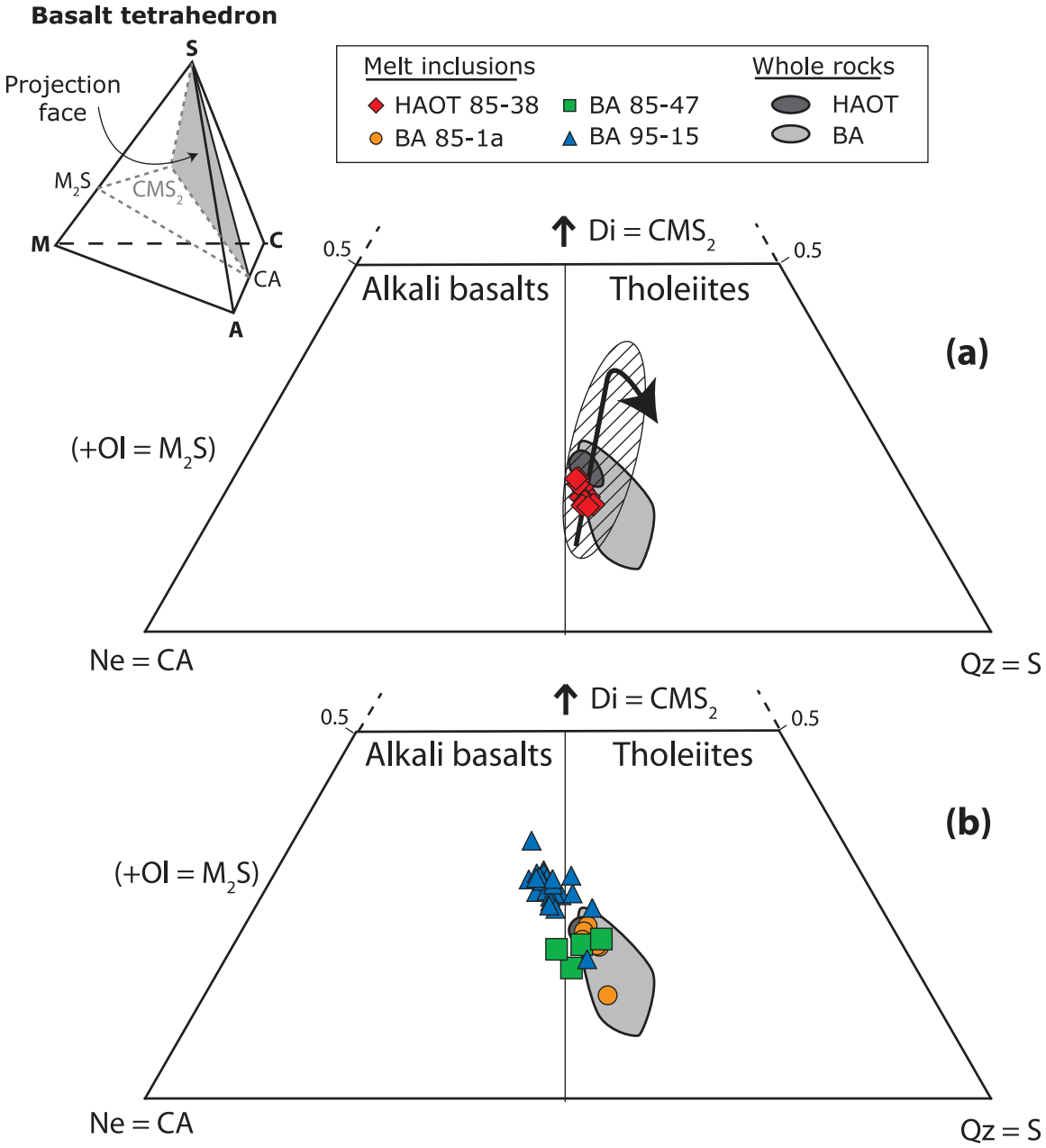

Fig. 7. Major element compositions of the HAOT melt inclusions (**a**) and BA melt inclusions (**b**). Data have been recalculated as CMAS components (O'Hara, 1968) using the following procedure: $C = (CaO - 10/3\ P_2O_5 + 2\ Na_2O + 2\ K_2O)$; $M = (MgO + FeO^* + MnO)$; $A = (Al_2O_3 + Na_2O + K_2O)$; $S = (SiO_2 - 2\ Na_2O - 2\ K_2O)$; then projected from olivine (M_2S) onto the Di–Ne–Qz (CMS_2–CA–S) face of the 'basalt tetrahedron' (Falloon & Green, 1988). Whole-rock compositions are from Baker *et al.* (1994) and Grove *et al.* (2002). Diagonally shaded area indicates experimental data for dry lherzolite melts at 10 and 15 kbar (MM3 from Baker & Stolper, 1994; Baker *et al.*, 1995; PHN1611 from Kushiro, 1996; HK66 from Hirose & Kushiro, 1993; Depma from Laporte *et al.*, 2004). The arrow represents an increase in the degree of melting. The HAOT melt inclusions (a) plot in the tholeiite field and fall in the compositional range of lherzolite melts. The BA melt inclusions (b) span a wider range of compositions, ranging from tholeiitic compositions close to the HAOT and BA lava compositions to alkali basalt-like compositions that are very different from the BA lava compositions.

Shasta lavas. Additional new information is given by the Cl and F contents of the melt inclusions. Assuming simple batch melting (using global partition coefficients during dry mantle melting of 0·0015 for Cl and 0·032 for F; Dalou *et al.*, 2009) and a degree of melting of ~10% [estimated following Grove *et al.* (2002), using average TiO_2 contents of the HAOT melt inclusions, a TiO_2 content of the mantle source of 0·12, and a bulk partition coefficient

for Ti of 0·062], the average Cl and F contents of the source mantle of the HAOT melt inclusions are 14 ± 4 ppm of F and 3 ± 1 ppm of Cl. These values are close to modelled values for the depleted source of primitive MORB (16 ± 3 ppm of F and $0{\cdot}9 \pm 0{\cdot}63$ ppm of Cl; Saal *et al.*, 2002).

Case of the BA melt inclusions

The BA melt inclusions are enriched in volatiles, alkalis and incompatible trace elements compared with the HAOT melt inclusions (Figs 4–6). These characteristics are typical of arc basalts. However, when recast into the CMAS system and projected from olivine onto the diopside–nepheline–quartz plane, the BA melt inclusions span a wider range of compositions than the HAOT melt inclusions (Fig. 7b), ranging from tholeiitic compositions close to the HAOT and the BA whole-rock compositions (Baker *et al.*, 1994; Grove *et al.*, 2002), to silica-undersaturated, alkali-rich compositions very different from the BA whole-rock compositions. The 85-1a and 85-47 melt inclusions (hypersthene-normative compositions) are closer to the tholeiitic end-member, whereas the 95-15 melt inclusions (nepheline-normative compositions) plot within the alkali basalt field. The silica-undersaturated, alkali-rich nature of many of the BA melt inclusions is atypical of arc magmas that often are silica-saturated. Although some ultracalcic, nepheline-normative liquids have been described in arc settings (Schiano *et al.*, 2000; Médard *et al.*, 2006), here the BA melt inclusions do not have ultracalcic compositions (i.e. CaO >13% and CaO/Al_2O_3 >1; Schiano *et al.*, 2000). This alkalic end-member is not expressed within the bulk-rock compositions of the host lavas, which are more evolved silica-saturated basaltic andesites, typical of convergent continental margins.

The BA lavas are thought to represent hydrous melts of a mantle source previously depleted by a melting episode and enriched with various amounts of slab-derived components (Baker *et al.*, 1994; Grove *et al.*, 2002). A similar petrogenesis can be inferred for the BA melt inclusions. The addition of slab-derived components enriched in water, alkalis and mobile elements to the source of the BA melt inclusions can account for their silica-undersaturated, alkali character. Mantle metasomatism results in the formation of hydrous minerals such as chlorite, amphibole or phlogopite in the mantle (Sen & Dunn, 1994; Ertan & Leeman, 1996). Several studies have shown that melting mantle enriched in amphibole or phlogopite can create silica-undersaturated, alkali-rich liquids (e.g. Holloway, 1973; Elkins-Tanton & Grove, 2003; Médard *et al.*, 2006). The trace element compositions of the BA melt inclusions support the hypothesis of a variable extent of metasomatism of the source. The 95-15 melt inclusions show a stronger enrichment in Cl, Ba, K, La, Sr, F and P than the 85-1a and 85-47 melt inclusions. Moreover, the temperatures of disappearance of the last daughter mineral in the BA melt inclusions (average of 1220°C for the melt inclusions from sample 95-15) are 100°C lower than those of the HAOT melt inclusions (1320°C on average), which is consistent with the lowering of the liquidus temperature of olivine in a basaltic melt by addition of 3 wt% water (Médard *et al.*, 2008). This temperature difference (100°C) is in good agreement with petrological estimations of the temperature of last equilibration with the upper mantle inferred from Shasta whole-rock compositions (1200°C for BA lavas, and 1300°C for HAOT lavas, Baker *et al.*, 1994). Based on these observations, the range of compositions observed in the BA melt inclusions may represent either mixing between melts from an nearly anhydrous mantle source (such as the 85-1a and 85-47 melt inclusions with low volatile contents) and melts from a metasomatized mantle source (such as the 95-15 silica-undersaturated, alkali- and volatile-rich melt inclusions), or melting of a hetrogeneous mantle after various degrees of metasomatism.

Alternative hypotheses for the origin of the compositional variation in the BA melt inclusions are: crustal contamination, magmatic processes such as the variation of degree of melting or crystallization, and finally binary mixing between primitive tholeiitic basalt, such as the HAOT melt inclusions, and evolved, dacite magmas (Streck *et al.*, 2007). First, as already shown for the bulk lava compositions (Fuis *et al.*, 1987; Baker *et al.*, 1991, 1994; Grove *et al.*, 2002), in the BA melt inclusions, the positive correlation of Ba with Sr (up to values of 740 and 880 ppm, respectively) is inconsistent with assimilation of a granitic crustal component. The assimilation of the Trinity ultramafic complex is expected to produce higher MgO and Cr contents than those measured in the BA lavas and melt inclusions (Baker *et al.*, 1994). Second, both variation in the degree of batch melting (of a depleted mantle) and variations in the degree of fractional crystallization (with an olivine–plagioclase–spinel–augite residue, Baker *et al*, 1994; Grove *et al.*, 2002) fail to reproduce the variation in fluid-mobile element compositions found in the BA lavas and melt inclusions. Third, it was postulated that the PMA lavas could represent mixing between the basaltic and the dacitic end-members of the Shasta lavas, combined with contamination with high-Mg country rocks (Streck *et al.*, 2007, 2008). A similar mixing origin could also be put forward for the origin of the enrichment of the BA melt inclusions. Unlike the PMA, we found that the major and trace element compositions of the BA melt inclusions intersect almost perpendicularly the mixing lines between a basaltic end-member and a dacitic end-member (inset in Fig. 8a). Therefore our preferred hypothesis remains that the BA melt inclusions represent hydrous melts from a mantle source containing various amounts of hydrous minerals (such as amphibole or phlogopite veins) formed by interaction with a slab-derived H_2O-rich component.

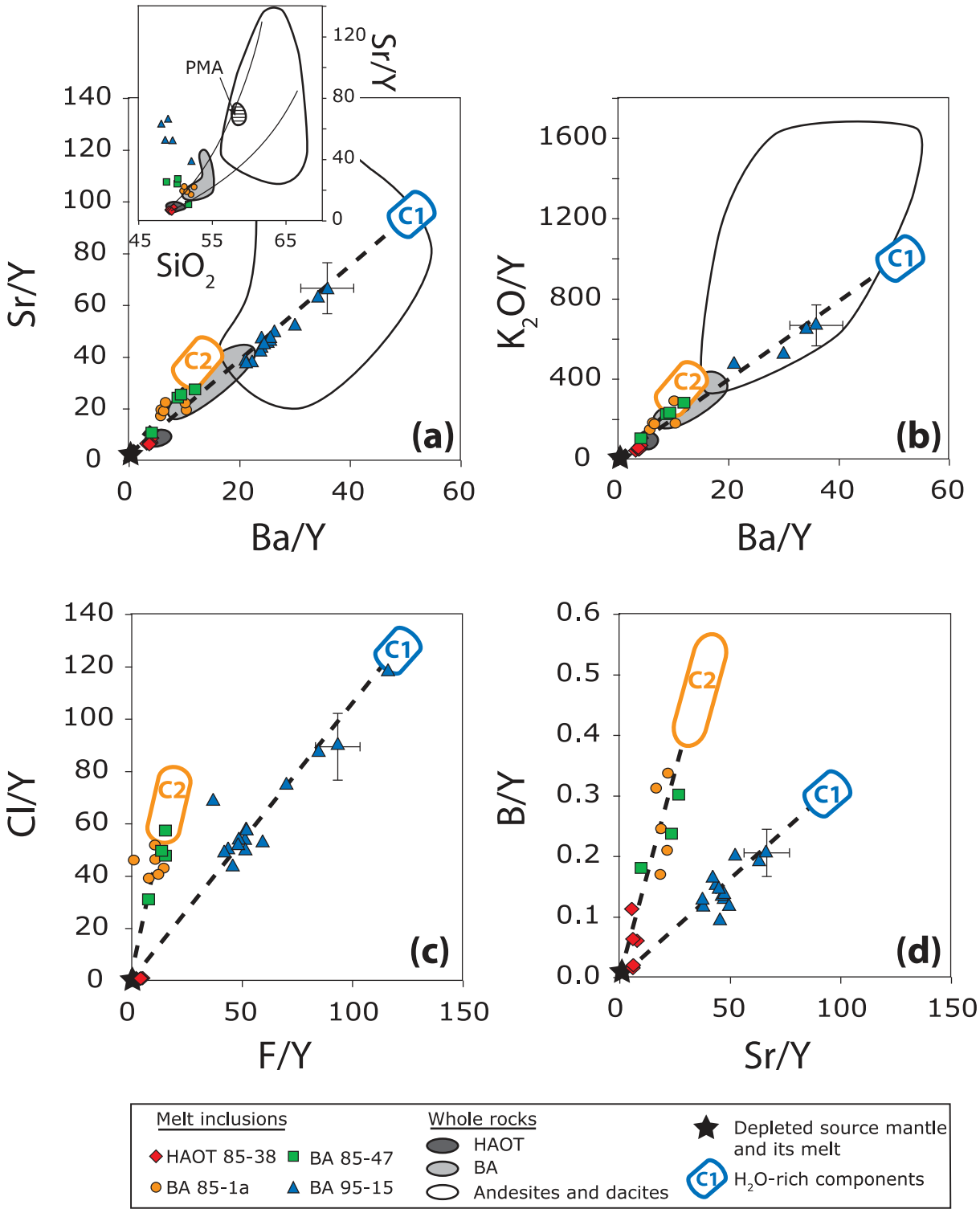

Fig. 8. Variations in (**a**) Ba/Y vs Sr/Y, (**b**) Ba/Y vs K_2O/Y, (**c**) Cl/Y vs F/Y and (**d**) Sr/Y vs B/Y for the Shasta melt inclusions. Error bars represent maximum errors on each ratio. Also shown in (a) and (b) are fields for the whole-rock Shasta lavas (Baker *et al.*, 1994; Grove *et al.*, 2002, 2005). In all four diagrams, the BA melt inclusion compositions can be reproduced by mixing between a depleted mantle source or melt (black star, Grove *et al.*, 2002) and one of the two H_2O-rich components (C1 for the 95-15 melt inclusions and C2 for the 85-1a and 85-47 melt inclusions). Inset in (a) shows Sr/Y vs SiO_2 variations in the Shasta melt inclusions (this study) and Shasta lavas (Baker *et al.*, 1994; Grove *et al.*, 2002, 2005). PMA, Primary magnesium-rich andesites. Curves represent mixing between a basaltic end-member and a dacitic end-member (Streck *et al.*, 2007). The trend of the 95-15 melt inclusions does not plot on the mixing lines of Streck *et al.* (2007); therefore the compositional variation of our inclusions cannot be explained by mixing between a basalt and a dacite.

The link between the BA melt inclusions and the lavas seems complex. The compositions of the BA lavas cannot be modelled using a simple crystallization model, starting from the compositions of the BA lavas. The aim of this discussion is to constrain the nature and origin of the BA melt inclusions. The relationship between the bulk-rock lavas and the inclusions certainly involves a complex combination of mixing, crystallization and crustal contamination, and is beyond the focus of this study. The following discussion focuses on the composition and the nature of the slab components that are responsible for the compositional variation of the BA melt inclusions.

Identification of the trace and volatile element compositions of the slab-derived H_2O-rich components using the melt inclusions

A characterization of the slab-derived components, in particular their volatile element compositions, can be directly obtained from the BA melt inclusion compositions. To this end, we investigated the variations of concentration ratios of incompatible elements, where the fluid-mobile element (K_2O, F, Cl, Li, B, Sr and Ba) is the numerator and the fluid-immobile element (Y, Zr, and Nb) is the denominator. According to the incompatibility of the two elements, such ratios minimize the effect of melting–crystallization processes and disclose the fluid effect in the mantle source of the inclusions. Although the variations of degree of melting and crystallization are probably responsible for some of the scatter within each group of Shasta melt inclusions, they cannot be solely responsible for the compositional variations of the trace element ratios between each group of melt inclusions. For instance, in Fig. 8, the variations in melt composition caused by varying the degree of melting of a depleted mantle source from 5 to 20% are always smaller than the error bars. We have systematically studied the correlations between all pairs of fluid-mobile element over immobile element ratios. In the following, we restrict the discussion to ratios involving Y because (1) the errors on Y contents (10%) are smaller than those on Nb contents (25%, because of the low Nb contents of the Shasta melt inclusions), and (2) the two groups of BA melt inclusions have the same range in Y contents (9–19 ppm), whereas they have different Zr contents (20–254 ppm for the 95-15 melt inclusions, and 25–57 ppm for the 85-1a and 85-47 melt inclusions). However, the main conclusions are still valid if Nb or Zr is considered instead of Y.

Key results of the trace element ratio correlation study are compiled in Fig. 8. The BA melt inclusion compositions can be divided into two groups, which plot on two mixing lines between the depleted source (black star at the bottom left corner of each graph) and one H_2O-rich component, C1 (for the 95-15 melt inclusion group) and C2 (for the 85-1a and 85-47 melt inclusion group), respectively. Although C1 and C2 show close Sr/Ba and K_2O/Ba ratios (Fig. 8a and b), their Cl/F and B/Sr ratios are clearly distinct (Fig. 8c and d), thus allowing the characterization of two distinct H_2O-rich components.

To determine the composition of these two H_2O-rich components, we used two different methods, one for trace elements and one for major and volatile elements. First, the trace element (Li, Sr, Y, Zr, Nb, Ba and La) concentrations of the H_2O-rich components were calculated using the flux melting model of Grove *et al.* (2002). This model comprises a mass-balance calculation, assuming that each trace element in the melt inclusions comes from two sources: (1) a silicate melt produced during batch melting of a mantle source that has been previously depleted by extraction of 6% melt, and (2) an H_2O-rich component derived from the subducted slab [see Grove *et al.* (2002) for more information about the source composition and the model parameters]. As explained above, the H_2O content of the BA melt inclusions is likely to be an underestimation of the primitive H_2O content of the melts because of early degassing. Therefore we decided to consider the water content of the primary BA magmas as that estimated experimentally (3·7 wt% for the 85-1a lava and 4·5 wt% for the 95-15 lava; Grove *et al.*, 2002) instead of the maximum melt inclusion H_2O contents of 2·4 wt% and 2·6 wt%, respectively. It should be noted, however, that this choice does not change our conclusions and by considering the maximum melt inclusion H_2O contents, the determination of the trace element concentrations in the C1 and C2 components would vary by only 10–20%. To estimate how enriched the H_2O-rich components are and to bracket the compositions of C1 and C2, we used both the most trace element poor and rich melt inclusions from each group of BA melt inclusions (i.e. melt inclusions 95-15 2J5 and 95-15 17 for C1, and melt inclusions 85-1a 1J9 and 85-1a 3G6 for C2). The minimum and maximum trace element compositions of the two components are reported in Table 5 and plotted in Fig. 9. C1 is enriched in Sr (6090–10 950 ppm) and Ba (3300–5070 ppm) but also Zr and La (800–1230 ppm and 130–250 ppm, respectively). Compared with C1, C2 is 2–4 times poorer in trace elements (Sr 2680–5160 ppm, Ba 890–1500 ppm, Zr 350–660 ppm, La 40–90 ppm). For each component, the maximum estimated composition of each element is approximately two times higher than the minimum estimated composition.

Second, we used a different approach to estimate the volatile and major element contents. As little is known about the halogen and B contents of the mantle wedge beneath Mt. Shasta, we used the correlations observed for each group of BA melt inclusions between volatile element and trace element concentration ratios (always using ratios normalized to Y, with estimated Y contents of the H_2O-rich components from Table 5; Fig. 8b–d).

Table 5: Minimum and maximum estimated compositions of the two H_2O-rich components C1 and C2

	$C1_{min}$	$C1_{max}$	$C2_{min}$	$C2_{max}$	Unit	Method
Inclusion:	95-15 2J5	95-15 17	85-1a 1J9	85-1a 3G6		
x:	7·70	7·70	6·00	6·00		
f:	0·2	0·18	0·14	0·08		
Li	80	58	61	76	ppm	1
Sr	6086	10952	2681	5162	ppm	1
Y	62	121	63	166	ppm	1
Zr	831	1266	350	664	ppm	1
Nb	23	57	10	24	ppm	1
Ba	3297	5871	892	1500	ppm	1
La	127	246	43	91	ppm	1
B	19	34	35	64	ppm	2
F	0·77	1·37	0·13	0·22	wt%	2
Cl	0·83	1·48	0·50	0·89	wt%	2
K_2O	7·87	14·02	3·18	5·06	wt%	2
Na_2O	20·21	36·77	23·16	39·98	wt%	2
H_2O	69·26	44·50	72·62	53·08	wt%	3
Cl/F	1·07	1·08	3·80	4·10		

The trace element compositions have been calculated using the flux melting model of Grove *et al*. (2002). This model consists of a mass-balance calculation, assuming that each trace element in the melt inclusions is contributed from two sources: (1) a silicate melt produced during batch melting of a mantle source that has been previously depleted by extraction of 6 wt% of melt, and (2) a H_2O-rich component derived from the slab (for more information about the model parameters, see Grove *et al.*, 2002). The melt inclusion composition is the silicate melt. Source compositions, partition coefficients and amount of fluid (*x*) are from Grove *et al*. (2002). Degree of melting (*f*) is estimated from TiO_2 contents of the melt inclusions, following Grove *et al*. (2002).
The B, F, Cl, K_2O and Na_2O compositions have been calculated using the equations of the regression lines from the correlations between the two groups of BA melt inclusions and the depleted mantle source and the Ba, Sr and Y contents of the H_2O-rich components calculated with method 1 (correlations of K_2O/Y vs Ba/Y, F/Y vs Ba/Y, Cl/Y vs Ba/Y and B/Y vs Sr/Y; regression coefficients for C1 are 0·99, 0·97, 0·94 and 0·90, respectively, and for C2 0·92, 0·77, 0·87 and 0·76, respectively).
H_2O contents are estimated by difference to 100%.

We calculated regression lines (1) between the depleted mantle source composition and the 95-15 melt inclusion compositions, and (2) between the depleted mantle source composition and the 85-1a and 85-47 melt inclusion compositions, respectively. Using the equations of the regression lines and the trace element contents of the two H_2O-rich components (previously determined by mass balance), we were able to calculate their Cl, F, B, K_2O and Na_2O contents (Table 5; Fig. 9). For example, we used the regression between Ba/Y and F/Y, together with the Ba and Y contents of each component to calculate their respective F contents. The regression coefficients were always better than 0·90 for Cl and 0·76 for C2, and for each element we obtained a range of concentrations corresponding to the spread of the inclusions along the Cl and C2 trends (Fig. 8). We found that Cl contains 20–37 wt% Na_2O, 8–14 wt% K_2O, 0·8–1·4 wt% F and 0·6–1·5 wt% Cl, whereas C2 contains 23–40 wt% Na_2O, 3–5 wt% K_2O, 0·1–0·2 wt% F and 0·5–0·9 wt% Cl (Table 5, Fig. 9). The water content (45–69 wt% for Cl, and 53–13 wt% for C2, Table 5) has been estimated by difference to 100%. Although they have not been estimated by the classical mass-balance approach, the major and volatile element compositions of Cl and C2 are within the same order of magnitude as the estimated H_2O-rich component reported for the Mariana subduction zone (44·1 wt% H_2O, 42·6 wt% Na_2O, 8·5 wt% K_2O and 1·2 wt% Cl; Stolper & Newman, 1994) and central Mexico subduction zone (47·7–49·5 wt% H_2O, 23·2–35·7 wt% Na_2O, 10·2–15·0 wt% K_2O and 1·0–1·6 wt% Cl; Cervantes & Wallace, 2003; Fig. 9).

Our model involves two slab-derived components (Cl and C2), with variable compositions (from Cl_{min} to Cl_{max} and from $C2_{min}$ to $C2_{max}$; Table 5). Two variations of this model can be considered. First, if we consider Cl and C2 with fixed compositions (equal to their most enriched end-members, Cl_{max} and $C2_{max}$), then the variations in the trace element compositions of the BA melt inclusions can be accounted for by a variation in the amount of each slab component added into the mantle source of the inclusions. In this case, a decrease of 50% in the amount of slab components added to the mantle source can reproduce the compositions of the melt inclusions with the lowest trace element contents. Second, using fixed Cl and C2 compositions, variation in the degree of melting may also result in the production of melts with variable trace element compositions. However, as stated above, small variations in the degree of melting within each group of the BA melt inclusions will account for only less than 10% of the variations in their trace element compositions.

Nature and source of the two H_2O-rich components

The contrasting compositions of the two groups of BA melt inclusions and their respective slab-derived components indicate several different sources and/or transport processes of these components. First, the three main fluxes that can carry volatile- and trace element-enriched phases are dehydration fluids, silicate melts and supercritical fluids. Our H_2O-rich components have estimated compositions that are enriched in H_2O (45–73 wt%) and fluid-mobile elements (B, Sr, K, etc.), as expected for a slab dehydration fluid. They are also enriched in fluid-immobile elements

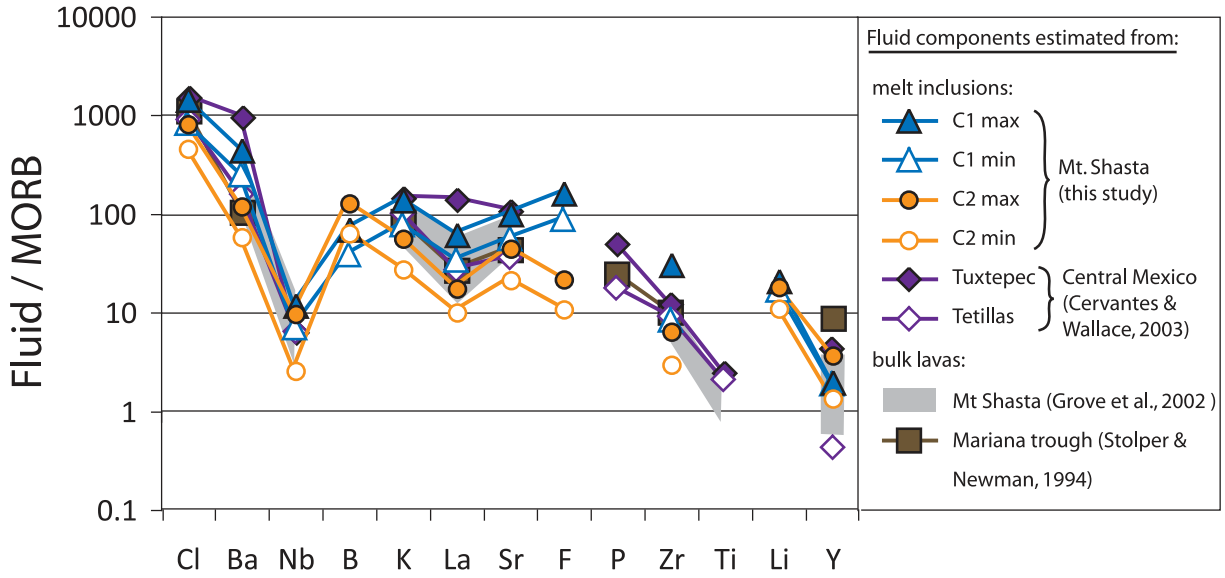

Fig. 9. Trace element compositions of the modelled H_2O-rich components C1 (triangles) and C2 (circles). C1 have variable compositions, especially rich in Cl, Ba and F, whereas C2 have lower trace element contents compared with C1. Also shown for comparison are the trace element compositions of the slab components estimated from Mt. Shasta lavas (shaded grey area, Grove *et al.*, 2002), from Mariana lavas (Stolper & Newman, 1994) and from central Mexico melt inclusions (Cervantes & Wallace, 2003). Fluid compositions are normalized to the average N-MORB composition (Hofmann, 1988; except for Cl and F, Saal *et al.*, 2002; B, Chaussidon & Marty, 1995; Li, Elliott *et al.*, 2004).

such as Nb, Y or Zr. This implies that the H_2O-rich components are different from typical 'cold' fluids formed during the dehydration of the slab reservoir, because such fluids are expected to be solute-poor (Brenan *et al.*, 1995). Moreover, both H_2O-rich components have low Cl/F ratios (C1 1·1; C2 4·0), hinting at a process such as melting, which does not significantly fractionate Cl relative to F, rather than dehydration that would fractionate these elements more strongly (Straub & Layne, 2003). The temperature of the slab beneath the volcanic arc for the young lithosphere subducted at 125 km depth beneath Mt. Shasta is likely to be warmer than 800°C (Peacock, 2004) which therefore favours melting of the subducted crust. However, the sediment and/or oceanic crust melts are thought to be silica-rich (Rapp & Watson, 1995; Johnson & Plank, 1999). Our model does not require a high SiO_2 content in the metasomatic components. Therefore C1 and C2 do not resemble pure slab melts either. The third possibility is a supercritical fluid component, which can carry both fluid-mobile and -immobile elements but has a lower SiO_2 content than slab melts (Johnson *et al.*, 1999; Kessel *et al.*, 2005). The slab beneath Mt. Shasta does not reach a depth corresponding to the high pressure required for the formation of such a supercritical fluid phase (6 GPa; Kessel *et al.*, 2005). Therefore, the best way to reproduce the chemical characteristics of our two H_2O components involves mixing between dehydration fluids and silicate melts. The result of this mixing could be a 'dense hydrous vapour' likely to be highly mobile in the mantle wedge (Stolper & Newman, 1994). Mixing is consistent with the results of a number of previous studies of the nature of slab-derived components in subduction zones (Johnson & Plank, 1999; Elliott, 2003; Le Voyer *et al.*, 2008; Johnson *et al.*, 2009).

The two main sources of H_2O-rich components in subduction zones are the subducted sediments and the altered oceanic crust (basalt). The two components carry different trace element, volatile element and $\delta^{11}B$ signatures; therefore they should come from reservoirs with contrasting compositions. Modelling of the boron isotopic variations during dehydration of the subducted slab allows us to constrain the origin of the H_2O-rich components (Fig. 10a). The sediments and altered oceanic crust are rich in boron (0–160 ppm for sediments, Ishikawa & Nakamura, 1993; 9–69 ppm for the altered oceanic crust, Spivack & Edmond, 1987) whereas the upper mantle is characterized by low boron concentrations (0·05 ppm; Chaussidon & Marty, 1995). The contrasting boron isotope compositions of altered oceanic crust ($\delta^{11}B$ from $+2{\cdot}2 \pm 0{\cdot}1$‰ to $+10{\cdot}6 \pm 0{\cdot}2$‰, Ishikawa & Nakamura, 1992) and sediments ($\delta^{11}B$ from $-6{\cdot}6 \pm 0{\cdot}1$‰ to $+4{\cdot}8 \pm 0{\cdot}1$‰ for non-carbonate lithologies; Ishikawa & Nakamura, 1993) allow us to discriminate between the relative contributions of these two reservoirs in the source of arc lavas. $\delta^{11}B$ can also trace slab transfer mechanisms because ^{11}B fractionates preferentially into aqueous fluids, whereas no fractionation occurs during partial melting (e.g. Palmer *et al.*, 1992). Melting of an unmetasomatized depleted MORB mantle

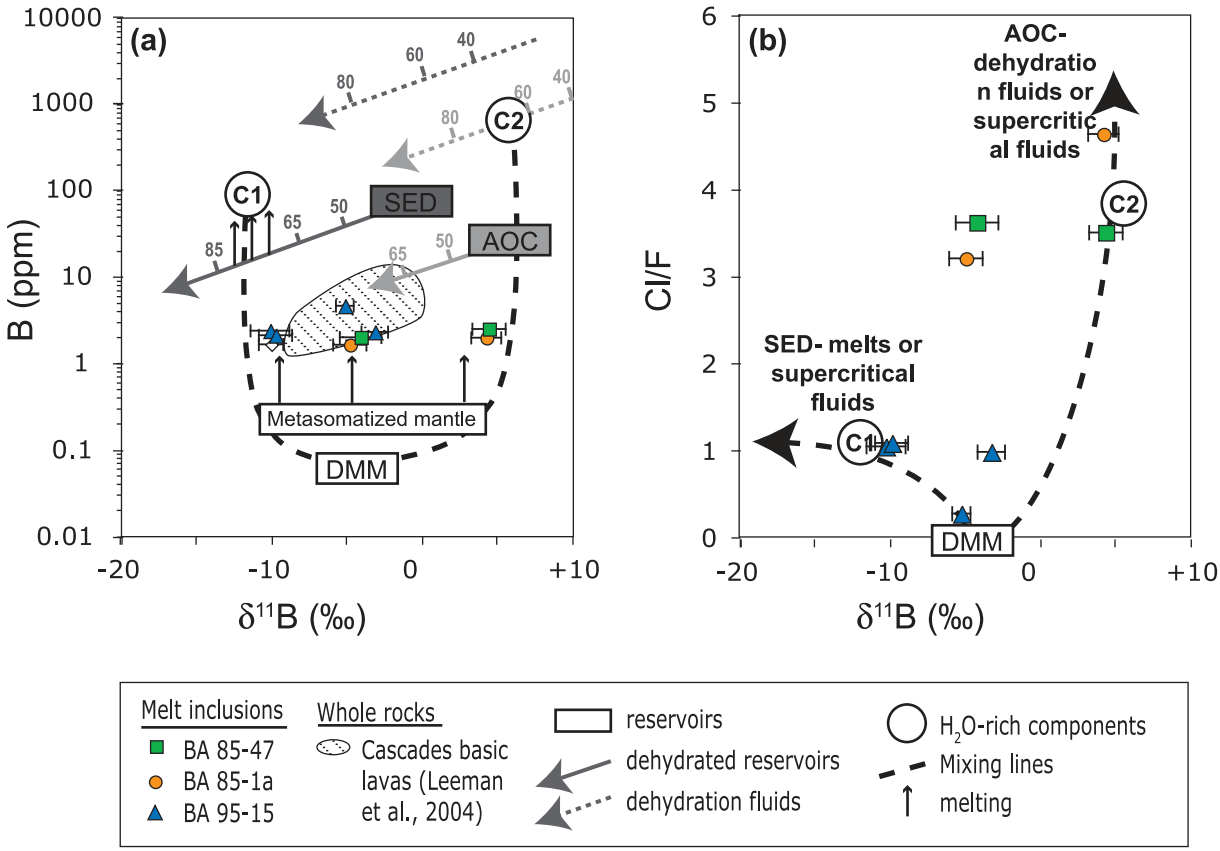

Fig. 10. (**a**) B content vs $\delta^{11}B$ for the BA melt inclusions. Error bars indicate the analytical errors associated with each $\delta^{11}B$ measurement ($\pm 1\sigma_m$). Also shown for comparison is the range for the basic lavas of the Cascades arc (diagonally shaded area; Leeman *et al.*, 2004) and the compositions of the main reservoirs (SED: sediments, 75 ppm B, $\delta^{11}B$ −1‰; AOC: altered oceanic crust, 26 ppm B, $\delta^{11}B$ +5·5‰; Leeman *et al.*, 2004; DMM: depleted MORB mantle, 0·05 ppm B, $\delta^{11}B$ −1‰; Chaussidon & Marty, 1995). The dehydration model is after Rose *et al.* (2001) and Le Voyer *et al.* (2008) and corresponds to a Rayleigh distillation model. Arrows starting from the SED and AOC reservoirs are theoretical trajectories of the residues during dehydration. Dotted arrows are the corresponding released fluids. Arrows are marked with the per cent of B loss during dehydration. We used a B partition coefficient between fluid and solid of 0·015 (You *et al.*, 1996) and a B isotopic fractionation between fluid and solid of +7‰ at 800°C (Williams *et al.*, 2001). Thin vertical arrows represent the theoretical evolution during melting of the corresponding reservoir (no isotopic fractionation; Palmer *et al.*, 1992). Bold dashed curves represent the mixing between the mantle and the two H_2O-rich components (Cl, dehydrated sediment melts; C2, dehydration fluids from the oceanic crust). (b) Variations in $\delta^{11}B$ and Cl/F of the BA melt inclusions. Estimated $\delta^{11}B$ for Cl and C2 are from (a); estimated Cl/F are from Table 5.

(DMM)-like mantle source ($\delta^{11}B$ of −4·0 ± 1·6‰; Chaussidon & Marty, 1995) fails to reproduce the wide range of $\delta^{11}B$ recorded in the BA melt inclusions (Fig. 10a). During progressive dehydration, the downgoing slab becomes less and less enriched in boron with an associated decrease in its $\delta^{11}B$ isotopic composition (Fig. 10a). At the same time, the released fluids are enriched in B compared with the residue (Fig. 10a). The first fluids released are extremely enriched in B as a result of the high mobility of B. The 95-15 melt inclusions ($\delta^{11}B$ from −10·2 ± 1·3‰ to −3·2 ± 0·9‰) have $\delta^{11}B$ values that are closer to those reported for the sediments that are subducted beneath the Cascades arc (−1‰; Leeman *et al.*, 2004); whereas the 85-1a and 85-47 melt inclusions ($\delta^{11}B$ from −4·9 ± 1·1‰ to +4·4 ± 1·1‰) have $\delta^{11}B$ values closer to those of the Juan de Fuca altered oceanic crust (+5·5‰; Leeman *et al.*, 2004; Fig. 10a). The range of $\delta^{11}B$ recorded in the BA melt inclusions is best reproduced by the melting of a mantle source that has been metasomatized by a mixture of sediment melts (corresponding to the Cl component) and dehydration fluids from the oceanic crust (corresponding to the C2 component; mixing lines in Fig. 10a). The required B contents of these two components are higher than those estimated using trace element correlations, showing that the primitive slab components may have been diluted by reaction with the surrounding mantle during the ascent (Grove *et al.*, 2002). The trace and volatile element compositions of the melt inclusions and of the slab-derived components also support this interpretation of the nature of the two H_2O-rich components: Cl is enriched in Ba, La, Cl, F and K_2O relative to C2, and, similarly, the sediments are enriched in these same

elements compared with the basaltic altered oceanic crust (Plank & Langmuir, 1998; Elliott, 2003; Straub & Layne, 2003). Our results emphasize that halogens in the melt inclusions may fingerprint the origin of the slab-derived components: our H_2O-rich components have Cl/F ratios (1·1 and 4·0) that are lower than estimated values for dehydration fluids (Cl/F of 9·5; Straub & Layne, 2003), because Cl/F in fluid is strongly fractionated (for example, seawater Cl/F ~15 000). The Cl/F values of the two H_2O-rich components are also higher than MORB values (0·1; Saal *et al.*, 2002) or pure slab melts (estimated Cl/F of 0·9; Straub & Layne, 2003). Moreover, our results show that sediment-derived components (Cl; Cl/F of 1·1) have lower Cl/F than oceanic-crust-derived components (C2; Cl/F of 4·0).

Flux melting vs decompression melting of hydrous mineral-bearing mantle?

We have shown that at least two H_2O-rich components are needed to account for the range in volatile and trace element compositions of the two groups of BA melt inclusions. However, it is unlikely that these two components are directly transferred from the slab to the mantle sources of Mt. Shasta magmas without any modification. In fact, the estimated range in composition of the two slab-derived components points towards a more complex origin. A key question is whether these components rise directly from the slab or if they are temporarily stored within hydrous minerals. For example, the addition of H_2O-rich components could have been significantly separated in time from the melting event leading to the generation of the Shasta basic magmas. This scenario was postulated by Leeman *et al.* (2005), to account for the variations in trace elements recorded in the Cascades lavas: the enrichment in mobile elements could reflect a 'stored' slab-derived component inherited from earlier stages of the Cascades subduction (Leeman *et al.*, 2005). However, lithium isotopic variations in the Mt. Shasta and Medicine Lake lavas (Magna *et al.*, 2006), as well as the $\delta^{11}B$ values of Shasta melt inclusions (this study), rather indicate the input of a 'modern' H_2O-rich component. The presence of a free fluid phase during mantle melting beneath Mt. Shasta has also been demonstrated by previous melting experiments and modelling (Baker *et al.*, 1994; Gaetani & Grove, 1998; Grove *et al.*, 2002). Conversely, the silica undersaturation of the BA melt inclusions suggests the involvement of hydrous minerals such as amphibole or phlogopite. Ultimately the two sources of volatiles (hydrous minerals and slab-derived fluid) are linked in that metasomatic minerals probably formed as a consequence of infiltrations of fluids from the subducted slab. Although the presence of H_2O-rich components during mantle melting beneath Mt. Shasta seems likely, there may have been an intermediate stage during which the slab components were stored within the mantle in hydrous minerals. Vigouroux *et al.* (2008) argued that the high-K lavas (3–8 wt% K_2O) from the Western Trans-Mexican Volcanic Belt result from the melting of a phlogopite-bearing mantle source. The K_2O contents of the Shasta BA melt inclusions are much lower (<1·1 wt%). Therefore, assuming the presence of hydrous minerals in the source of the BA melt inclusions, amphibole would be more likely than phlogopite. In the case of an amphibole-bearing mantle source, several melting scenarios are possible: (1) flux melting of amphibole-bearing mantle by a continuous input of slab-derived components; (2) down-dragging of the amphibole-bearing mantle at the interface with the slab and melting as a result of amphibole breakdown; (3) upwelling and decompression melting of amphibole-bearing mantle. In the last scenario, amphibole would be one of the first minerals to melt. The resultant hydrous melts would carry the slab signature and enhance melting of the surrounding mantle.

CONCLUSIONS

The study of olivine-hosted primary melt inclusions provides new information about the petrogenesis of the primary magmas of Mt. Shasta. The melt inclusion compositions fall on the primitive extension of the trend of the lavas' compositions: they have lower SiO_2 contents and higher MgO contents compared with the basic lavas. The BA melt inclusions are enriched in incompatible elements and fluid-mobile elements. They display a stronger signature of slab-derived components than the basic lavas, in which the H_2O-rich component signature is diluted. Previous experimental studies on the Mt. Shasta lavas have provided evidence for the formation of both dry (HAOT lavas) and wet (BA lavas) melts (Baker *et al.*, 1994; Grove *et al.*, 2002). Our new results from the Mt. Shasta melt inclusions support this interpretation: the HAOT melt inclusions have low and clustered volatile compositions, whereas the BA melt inclusions have higher and more variable volatile compositions. The trace element enrichment of the BA melt inclusions cannot be reproduced by magmatic processes, crustal contamination or mixing with the dacitic magma end-member of Mt. Shasta and requires the addition of slab-derived components to a depleted mantle source. The selective enrichment in fluid-mobile elements such as K, F, Cl, Ba and B shows the imprints of two slab-derived components. These two components are rich in fluid-mobile elements but also in incompatible trace elements. Their Cl/F and the $\delta^{11}B$ of the melt inclusions indicate that they represent mixing between sediment melts and dehydration fluids from the altered oceanic crust.

FUNDING

This study was supported by a French Agence Nationale de la Recherche «Jeune Chercheur» grant (2006, Centre

National de la Recherche Scientifique, France) to E. F. Rose-Koga, and by a student travel grant from Ecole Doctorale des Sciences Fondamentales (Université Blaise Pascal, Clermont-Ferrand, France) to M. Le Voyer.

ACKNOWLEDGEMENTS

This study has benefited from constructive discussions with K. T. Koga, E. Médard, S. Lambart, C. Dalou and J. Barr. Special thanks go to J.-L. Devidal, J.-M. Hénot and N. Cluzel for their invaluable help with electron microprobe, MEB and microscope heating stage, respectively. We also thank P. J. Wallace, A. E. Saal, M. J. Streck and an anonymous reviewer for their thorough and helpful reviews that led to many improvements in the final manuscript.

REFERENCES

Alletti, M., Baker, D. R. & Freda, C. (2007). Halogen diffusion in a basaltic melt. *Geochimica et Cosmochimica Acta* **71**, 3570–3580.

Anderson, A. T. (1973). The before-eruption water content of some high-alumina magmas. *Bulletin of Volcanology* **37**, 530–522.

Anderson, A. T. (1974*a*). Chlorine, sulfur and water in magmas and oceans. *Geological Society of America Bulletin* **85**, 1485–1492.

Anderson, A. T. (1974*b*). Evidence for a picritic, volatile-rich magma beneath Mt. Shasta, California. *Journal of Petrology* **15**, 243–267.

Anderson, A. T. (1976). Magma mixing: petrological process and volcanological tool. *Journal of Volcanology and Geothermal Research* **1**, 3–33.

Anderson, A. T. (1979). Water in some hypersthenic magmas. *Journal of Geology* **87**, 509–531.

Baker, M. B. (1988). *Evolution of lavas at Mt. Shasta volcano, N. California: an experimental and petrological study.* Boston, MA: PhD thesis, MIT, 356 p.

Baker, M. B. & Stolper, E. M. (1994). Determining the composition of high-pressure mantle melts using diamond aggregates. *Geochimica et Cosmochimica Acta* **58**, 2811–2827.

Baker, M. B., Grove, T. L., Kinzler, R. J., Donnelly-Nolan, J. M. & Wandless, G. A. (1991). Origin of compositional zonation (high-alumina basalt to basaltic andesite) in the Giant Crater lava field, Medicine Lake volcano, northern California. *Journal of Geophysical Research* **96**, 21819–21842.

Baker, M. B., Grove, T. L. & Price, R. (1994). Primitive basalts and andesites from the Mt. Shasta region, N. California: products of varying melt fraction and water content. *Contributions to Mineralogy and Petrology* **118**, 111–129.

Baker, M. B., Hirschmann, M. M., Ghiorso, M. S. & Stolper, E. M. (1995). Composition of near-solidus peridotite melts from experiments and thermodynamic calculations. *Nature* **375**, 308–311.

Barr, J. A., Grove, T. L. & Elkins-Tanton, L. T. (2007). Comment on 'High-magnesian andesites from Mount Shasta: a product of magma mixing and contamination, not a primitive melt' Streck, M. J., Leeman, W. P., Chelsey, J. *Geology* **35**, e147–e148.

Barr, J. A., Grove, T. L. & Carlson, R. W. (2008). Primitive subduction zone magmatism at Mt. Shasta, California: Geochemical and petrologic characteristics of hydrous mantle derived melts. *EOS Transactions, American Geophysical Union, Fall Meeting Supplement* **89**, Abstract V33C-2226.

Bartels, K. S., Kinzler, R. J. & Grove, T. L. (1991). High pressure phase relations of primitive high-alumina basalts from Medicine Lake volcano, northern California. *Contributions to Mineralogy and Petrology* **108**, 253–270.

Benjamin, E. R., Plank, T., Wade, J. A., Kelley, K. A., Hauri, E. H. & Alvarado, G. E. (2007). High water contents in basaltic magmas from Iraz Volcano, Costa Rica. *Journal of Volcanology and Geothermal Research* **168**, 68–92.

Bertagnini, A., Métrich, N., Landi, P. & Rosi, M. (2003). Stromboli volcano (Aeolian Archipelago, Italy): An open window on the deep-feeding system of a steady state basaltic volcano. *Journal of Geophysical Research* **108**, doi:10.1029/2002JB002146.

Bouvier, A.-S., Métrich, N. & Deloule, E. (2008). Slab-derived fluids in the magma sources of St. Vincent (Lesser Antilles arc): Volatile and light element imprints. *Journal of Petrology* **49**, 1427–1448.

Brenan, H. F., Shaw, J. M., Reyrson, D. L. & Phinney, (1995). Mineral–aqueous fluid partitioning of trace elements at 900°C and 2·0 GPa: constraints on the trace element chemistry of mantle and deep crustal fluids. *Geochimica et Cosmochimica Acta* **59**, 3331–3350.

Cervantes, P. & Wallace, P. J. (2003). Role of H_2O in subduction-zone magmatism: New insights from melt inclusions in high-Mg basalts from central Mexico. *Geology* **31**, 235–238.

Chaussidon, M. & Marty, B. (1995). Primitive boron isotope composition of the mantle. *Science* **269**, 383–386.

Christiansen, R. L., Kleinhampl, F. J., Blakely, R. J., Tuchek, E. T., Johnson, F. L. & Conyac, M. D. (1977). Resource appraisal of the Mt. Shasta wilderness study area, Siskiyou County, California. *US Geological Survey, Open-file Report* **53**, 77–250.

Conrey, R. M., Sherrod, D. R., Hooper, P. R. & Swanson, D. A. (1997). Diverse primitive magmas in the Cascade arc, northern Oregon and southern Washington. *Canadian Mineralogist* **35**, 367–396.

Cottrell, E., Spiegelman, M. & Langmuir, C. H. (2002). Consequences of diffusive reequilibration for the interpretation of melt inclusions. *Geochemistry, Geophysics, Geosystems* **3**, doi:10.1029/2001GC000205.

Cross, W., Iddings, J. P., Pirsson, L. V. & Washington, H. S. (1903). *Quantitative Classification of Igneous Rocks*. Chicago, IL: University of Chicago Press.

Dalou, C., Koga, K. T. & Shimizu, N. (2009). Chlorine and fluorine partitioning between peridotite and basalt at mantle wedge conditions: Implications for arc magma source, AGU Fall Meeting.

Danyushevsky, L. V., Della-Pasqua, F. N. & Sokolov, S. (2000). Re-equilibration of melt inclusions trapped by magnesian olivine phenocrysts from subduction-related magmas: petrological implications. *Contributions to Mineralogy and Petrology* **138**, 68–83.

Danyushevsky, L. V., McNeill, A. W. & Sobolev, A. V. (2002). Experimental and petrological studies of melt inclusions in phenocrysts from mantle-derived magmas: an overview of techniques, advantages and complications. *Chemical Geology* **183**, 5–24.

Elkins-Tanton, L. T. & Grove, T. L. (2003). Evidence for deep melting of hydrous metasomatized mantle: Pliocene high-potassium magmas from the Sierra Nevada. *Journal of Geophysical Research* **108**, 1–18.

Elliott, T. (2003). Tracers of the slab. In: Eiler, J. M. (ed.) *Inside the Subduction Factory. Geophysical Monograph, American Geophysical Union* **138**, 23–43.

Elliott, T., Jeffcoate, A. & Bouman, C. (2004). The terrestrial Li isotope cycle: light-weight constraints on mantle convection. *Earth and Planetary Science Letters* **220**, 231–245.

Ertan, I. E. & Leeman, W. P. (1996). Metasomatism of Cascades subarc mantle: evidence from a rare phlogopite orthopyroxenite xenolith. *Geology* **24**, 77–105.

Fahey, A. J., Zinner, E. K., Crozaz, G. & Kornacki, A. S. (1987). Microdistributions of Mg isotopes and REE abundances in a Type A calcium–aluminum-rich inclusion from Efremovka. *Geochimica et Cosmochimica Acta* **51**, 3215–3229.

Falloon, T. J. & Green, D. H. (1988). Anhydrous partial melting of peridotite from 8 to 35 kb and the petrogenesis of MORB. *Journal of Petrology* **29**, 379–414.

Faure, F. & Schiano, P. (2005). Experimental investigation of equilibration conditions during forsterite growth and melt inclusion formation. *Earth and Planetary Science Letters* **236**, 882–898.

Fuis, G. S., Zucca, J. J., Mooney, W. D. & Milkereit, B. (1987). A geologic interpretation of seismic-refraction results in northeastern California. *Geological Society of America Bulletin* **98**, 53–65.

Gaetani, G. A. & Grove, T. L. (1998). The influence of water on melting of mantle peridotite. *Contributions to Mineralogy and Petrology* **131**, 323–346.

Gill, J. G. (1981). *Orogenic Andesites and Plate Tectonics*. New York: Springer.

Gioncada, A., Clocchiatti, R., Sbrana, A., Bottazzi, P., Massare, D. & Ottolini, L. (1998). A study of melt inclusions at Vulcano (Aeolian Islands, Italy): insights on the primitive magmas and on the volcanic feeding system. *Bulletin of Volcanology* **60**, 286–306.

Green, N. L. & Harry, D. L. (1999). On the relationship between subducted slab age and arc basalt petrogenesis, Cascadia subduction system, North America. *Earth and Planetary Science Letters* **171**, 367–381.

Grove, T. L., Parman, S. W., Bowring, S. A., Price, R. C. & Baker, M. B. (2002). The role of an H_2O-rich fluid component in the generation of primitive basaltic andesites and andesites from the Mt. Shasta region, N California. *Contributions to Mineralogy and Petrology* **142**, 375–396.

Grove, T. L., Elkins-Tanton, L. T., Parman, S. W., Chatterjee, N., Müntener, O. & Gaetani, G. A. (2003). Fractional crystallization and mantle-melting controls on calc-alkaline differentiation trends. *Contributions to Mineralogy and Petrology* **145**, 515–533.

Grove, T. L., Baker, M. B., Price, R. C., Parman, S. W., Elkins-Tanton, L. T., Chatterjee, N. & Müntener, O. (2005). Magnesian andesite and dacite lavas from Mt. Shasta, northern California: products of fractional crystallization of H_2O-rich mantle melts. *Contributions to Mineralogy and Petrology* **148**, 542–565.

Hauri, E. (2002). SIMS analysis of volatiles in silicate glasses, 2: isotopes and abundances in Hawaiian melt inclusions. *Chemical Geology* **183**, 115–141.

Hirose, K. & Kushiro, I. (1993). Partial melting of dry peridotites at high pressures: Determination of compositions of melts segregated from peridotite using aggregates of diamond. *Earth and Planetary Science Letters* **114**, 477–489.

Hofmann, A. W. (1988). Chemical differentiation of the Earth: the relationship between mantle, continental crust, and oceanic crust. *Earth and Planetary Science Letters* **90**, 297–314.

Holloway, J. R. (1973). The system pargasite–H_2O–CO_2: a model for melting of a hydrous mineral with a mixed-volatile fluid—I. Experimental results to 8 kbar. *Geochimica et Cosmochimica Acta* **37**, 651–666.

Ishikawa, T. & Nakamura, E. (1992). Boron isotope geochemistry of the oceanic crust from DSDP/ODP Hole 504B. *Geochimica et Cosmochimica Acta* **56**, 1633–1639.

Ishikawa, T. & Nakamura, E. (1993). Boron isotope systematics of marine sediments. *Earth and Planetary Science Letters* **117**, 567–580.

Jarosewich, E., Parkes, A. S. & Wiggins, L. B. (1979). Microprobe analyses of four natural glasses and one mineral: an interlaboratory study of precision and accuracy. *Smithsonian Contributions to the Earth Sciences* **22**, 53–67.

Jicha, B., Hart, G., Johnson, C., Hildreth, W., Beard, B., Shirey, S. & Valley, J. (2009). Isotopic and trace element constraints on the petrogenesis of lavas from the Mount Adams volcanic field, Washington. *Contributions to Mineralogy and Petrology* **157**, 189–207.

Jochum, K. P., Stoll, B. *et al*. (2006). MPI-DING reference glasses for *in situ* microanalysis: New reference values for element concentrations and isotope ratios. *Geochemistry, Geophysics, Geosystems* **7**, doi:10.1029/2005GC001060.

Johnson, M. C. & Plank, T. (1999). Dehydration and melting experiments constrain the fate of subducted sediments. *Geochemistry, Geophysics, Geosystems* **1.**

Johnson, E. R., Wallace, P. J., Delgano Granados, H., Manea, V. C., Kent, A. J. R., Bindeman, I. N. & Donegan, C. S. (2009). Subduction-related volatile recycling and magma generation beneath central Mexico: Insights from melt inclusions, oxygen isotopes and geodynamical models. *Journal of Petrology* **50**, 1729–1764.

Jugo, P. J., Luth, R. W. & Richards, J. P. (2005). Experimental data on the speciation of sulfur as a function of oxygen fugacity in basaltic melts. *Geochimica et Cosmochimica Acta* **69**, 497–503.

Kamenetsky, V. & Clocchiatti, R. (1996). Primitive magmatism of Mt. Etna: insights from mineralogy and melt inclusions. *Earth and Planetary Science Letters* **142**, 553–572.

Kessel, R., Schmidt, M. W., Ulmer, P. & Pettke, T. (2005). Trace element signature of subduction-zone fluids, melts and supercritical liquids at 120–180 km depth. *Nature* **437**, 724–727.

Kushiro, I. (1996). Partial melting of a fertile mantle peridotite at high pressures: an experimental study using aggregates of diamond. In: Basu, A. & Hart, S. (eds) *Earth Processes: Reading the Isotopic Code. Geophysical Monograph, American Geophysical Union* **95**, 109–022.

Laporte, D., Toplis, M. J., Seyler, M. & Devidal, J.-L. (2004). A new experimental technique for extracting liquids from peridotite at very low degrees of melting: application to partial melting of depleted peridotite. *Contributions to Mineralogy and Petrology* **146**, 463–384.

Laubier, M., Schiano, P., Doucelance, R., Ottolini, L. & Laporte, D. (2007). Olivine-hosted melt inclusions and melting processes beneath the FAMOUS zone (Mid-Atlantic Ridge). *Chemical Geology* **240**, 129–150.

Le Voyer, M. (2009). Rôle des fluides dans la genèse des magmas d'arcs: analyses in situ des éléments volatils et des isotopes du bore dans les inclusions magmatiques des olivines primitives. Clermont-Ferrand: PhD thesis, Blaise Pascal University, 276 p.

Le Voyer, M., Rose-Koga, E. F., Laubier, M. & Schiano, P. (2008). Petrogenesis of arc lavas from the Rucu Pichincha and Pan de Azucar volcanoes (Ecuadorian arc): Major, trace element, and boron isotope evidences from olivine-hosted melt inclusions. *Geochemistry, Geophysics, Geosystems* **9**, doi:10.1029/2008GC002173.

Leeman, W. P., Tonarini, S., Chan, L. H. & Borg, L. E. (2004). Boron and lithium isotopic variations in a hot subduction zone—the southern Washington Cascades. *Chemical Geology* **212**, 101–124.

Leeman, W. P., Lewis, J. F., Evarts, R. C., Conrey, R. M. & Streck, M. J. (2005). Petrologic constraints on the thermal structure of the Cascades arc. *Journal of Volcanology and Geothermal Research* **140**, 67–105.

Luhr, J. F. & Haldar, D. (2006). Barren Island Volcano (NE Indian Ocean): Island-arc high-alumina basalts produced by troctolite contamination. *Journal of Volcanology and Geothermal Research* **149**, 177–212.

MacDonald, G. A. (1966). Geology of the Cascade Range and Modoc Plateau. In: Bailey, E. H. (ed.) *Geology of Northern California. California Division of Mines Bulletin* **190**, 65–95.

Magna, T., Wiechert, U., Grove, T. L. & Halliday, A., N. (2006). Lithium isotope fractionation in the southern Cascadia subduction zone. *Earth and Planetary Science Letters* **250**, 428–443.

Massare, D., Métrich, N. & Clocchiatti, R. (2002). High-temperature experiments on silicate melt inclusions in olivine at 1 atm: inference on temperatures of homogenization and H_2O concentrations. *Chemical Geology* **183**, 87–98.

Mathez, E. A. & Webster, J. D. (2005). Partitioning behavior of chlorine and fluorine in the system apatite–silicate melt–fluid. *Geochimica et Cosmochimica Acta* **69**, 1275–1286.

Médard, E. & Grove, T. (2008). The effect of H_2O on the olivine liquidus of basaltic melts: experiments and thermodynamic models. *Contributions to Mineralogy and Petrology* **155**, 417–432.

Médard, E., Schmidt, M. W., Schiano, P. & Ottolini, L. (2006). Melting of amphibole-bearing wehrlites; an experiment study on the origin of ultra-calcic nepheline-normative melts. *Journal of Petrology* **47**, 481–504.

Métrich, N. & Wallace, P. J. (2008). Volatile abundances in basaltic magmas and their degassing paths tracked by melt inclusions. In: Putirka, K. D. & Tepley, F. J., III (eds) *Minerals, Inclusions and Volcanic Processes. Mineralogical Society of America and Geochemical Society, Reviews in Mineralogy and Geochimistry* **69**, 364–402.

Métrich, N., Clocchiatti, R., Mosbah, M. & Chaussidon, M. (1993). The 1989–1890 activity of Etna. Magma mingling and ascent of a H_2O–Cl–S rich basaltic magma. Evidence from melt inclusions. *Journal of Volcanology and Geothermal Research* **59**, 131–144.

Métrich, N., Allard, P., Spilliaert, N., Andronico, D. & Burton, M. (2004). 2001 flank eruption of the alkali- and volatile-rich primitive basalt responsible for Mount Etna's evolution in the last three decades. *Earth and Planetary Sciences Letters* **224**, 1–17.

Newman, S. & Lowenstern, J. B. (2002). VC: a silicate melt–H_2O–CO_2 solution model written in Visual Basic for Excel. *Computers and Geosciences* **28**, 597–604.

O'Hara, M. J. (1968). The bearing of phase equilibria studies in synthetic and natural systems on the origin and evolution of basic and ultrabasic rocks. *Earth-Science Reviews* **4**, 60–133.

Palmer, M. R., Spivack, A. J. & Edmond, J. M. (1987). Temperature and pH controls over isotopic fractionation during adsorption of boron on marine clay. *Geochimica et Cosmochimica Acta* **51**, 2319–2323.

Palmer, M. R., London, D., Morgan, V. & Babb, H. A. (1992). Experimental determination of fractionation of $^{11}B/^{10}B$ between tourmaline and aqueous vapor: A temperature- and pressure-dependent isotopic system. *Chemical Geology* **101**, 123–129.

Peacock, S. M. (2004). Thermal Structure and Metamorphic Evolution of Subducting Slabs. In: Eiler, J. (ed.) *Inside the Subduction Factory. Geophysical Monograph, American Geophysical Union* **138**, 7–22.

Peacock, S. M. & Hervig, R. L. (1999). Boron isotopic composition of subduction-zone metamorphic rocks. *Chemical Geology* **160**, 281–290.

Peate, D. W. & Pearce, J. A. (1998). Causes of spatial compositional variations in Mariana arc lavas: Trace element evidence. *Island Arc* **7**, 479–495.

Peccerillo, P. & Taylor, S. R. (1976). Geochemistry of Eocene calc-alkaline volcanic rocks from the Kastamonu area, northern Turkey. *Contributions to Mineralogy and Petrology* **58**, 63–81.

Pilet, S., Baker, M. B. & Stolper, E. M. (2007). Experimental constraints on the origin of OIBs. *Geophysical Research Abstracts* **9**, 04613.

Plank, T. & Langmuir, C. H. (1998). The chemical composition of subducting sediment and its consequences for the crust and mantle. *Chemical Geology* **145**, 325–394.

Portnyagin, M., Hoernle, K., Plechov, P., Mironov, N. & Khubunaya, S. (2007). Constraints on mantle melting and composition and nature of slab components in volcanic arcs from volatiles (H_2O, S, Cl, F) and trace elements in melt inclusions from the Kamchatka Arc. *Earth and Planetary Science Letters* **255**, 53–69.

Rapp, R. P. & Watson, E. B. (1995). Dehydration melting of metabasalt at 8–32 kbar: Implications for continental growth and crust–mantle recycling. *Journal of Petrology* **36**, 891–931.

Righter, K. (2000). A comparison of basaltic volcanism in the Cascades and western Mexico: compositional diversity in continental arcs. *Tectonophysics* **318**, 99–117.

Roedder, E. (ed.) (1984). *Fluid Inclusions. Mineralogical Society of America, Reviews in Mineralogy* **12**.

Roggensack, K., Hervig, R. L., McKnight, S. B. & Williams, S. N. (1997). Explosive basaltic volcanism from Cerro Negro volcano: Influence of volatiles on eruptive style. *Science* **12**, 1639–1642.

Rose, E. F., Shimizu, N., Layne, G. D. & Grove, T. L. (2001). Melt production beneath Mt. Shasta from boron data in primitive melt inclusions. *Science* **293**, 281–283.

Rose-Koga, E. F., Shimizu, N., Devidal, J.-L., Koga, K. T., Le Voyer, M. & Döbeli, M. (2008). Investigation of F, S and Cl standards by ion probe and electron microprobe. *EOS Transactions, American Geophysical Union, Fall Meeting Supplement* **89**, Abstract V31B-2145.

Saal, A. E., Hauri, E. H., Langmuir, C. H. & Perfit, M. R. (2002). Vapour undersaturation in primitive mid-ocean-ridge basalt and the volatile content of Earth's upper mantle. *Nature* **419**, 451–455.

Schiano, P. (2003). Primitive mantle magmas recorded as silicate melt inclusions in igneous minerals. *Earth-Science Reviews* **63**, 121–144.

Schiano, P. & Bourdon, B. (1999). On the preservation of mantle information in ultramafic nodules: glass inclusions within minerals versus interstitial glasses. *Earth and Planetary Science Letters* **169**, 173–188.

Schiano, P., Eiler, J. M., Hutcheon, I. D. & Stolper, E. M. (2000). Primitive CaO-rich, silica-undersaturated melts in island arcs: Evidence for the involvement of clinopyroxene-rich lithologies in the petrogenesis of arc magmas. *Geochemistry, Geophysics, Geosystems* **1**, doi:10.1029/1999GC000032.

Schiano, P., Clocchiatti, R., Ottolini, L. & Sbrana, A. (2004). The relationship between potassic, calc-alkaline and Na-alkaline magmatism in South Italy volcanoes: A melt inclusion approach. *Earth and Planetary Science Letters* **220**, 121–137.

Schmidt, M. E., Grunder, A. L. & Rowe, M. C. (2008). Segmentation of the Cascade Arc as indicated by Sr and Nd isotopic variation among diverse primitive basalts. *Earth and Planetary Science Letters* **266**, 166–181.

Sen, C. & Dunn, T. (1994). Dehydration melting of a basaltic composition amphibolite at 1·5 and 2·0 GPa: implications for the origin of adakites. *Contributions to Mineralogy and Petrology* **117**, 394–409.

Severs, M. J., Azbej, T., Thomas, J. B., Mandeville, C. W. & Bodnar, R. J. (2007). Experimental determination of H_2O loss from melt inclusions during laboratory heating: Evidence from Raman spectroscopy. *Chemical Geology* **237**, 358–371.

Shimizu, K., Shimizu, N., Komiya, K., Suzuki, K., Maruyama, S. & Tatsumi, Y. (2009). CO_2-rich komatiitic melt inclusions in Cr-spinels within beach sand from Gorgona Island, Colombia. *Earth and Planetary Science Letters* **299**, 33–43.

Sisson, T. W. & Grove, T. L. (1993). Experimental investigations of the role of H_2O in calc-alkaline differentiation and subduction zone magmatism. *Contributions to Mineralogy and Petrology* **113**, 143–166.

Smith, D. R. & Leeman, W. P. (2005). Chromian spinel–olivine phase chemistry and the origin of primitive basalts of the southern Washington Cascades. *Journal of Volcanology and Geothermal Research* **140**, 49–66.

Sobolev, A. V. & Chaussidon, M. (1996). H_2O concentrations in primary melts from supra-subduction zones and mid-ocean ridges:

Implications for H_2O storage and recycling in the mantle. *Earth and Planetary Science Letters* **137**, 45–55.

Sobolev, A. V. & Danyushevsky, L. V. (1994). Petrology and geochemistry of boninites from the north termination of the Tonga Trench: constraints on the generation conditions of primary high-Ca boninite magmas. *Journal of Petrology* **35**, 1183–1213.

Spandler, C., O'Neill, H. S. C. & Kamenetsky, V. S. (2007). Survival times of anomalous melt inclusions from element diffusion in olivine and chromite. *Nature* **447**, 303–306.

Spilliaert, N., Métrich, N. & Allard, P. (2006). S–Cl–F degassing pattern of water-rich alkali basalt: Modelling and relationship with eruption styles on Mount Etna volcano. *Earth and Planetary Science Letters* **248**, 772–786.

Spivack, A. J. & Edmond, J. M. (1987). Boron isotope exchange between seawater and the oceanic crust. *Geochimica et Cosmochimica Acta* **51**, 1033–1043.

Stolper, E. M. & Newman, S. (1994). The role of water in the petrogenesis of Mariana trough magmas. *Earth and Planetary Science Letters* **121**, 293–325.

Straub, S. M. & Layne, G. D. (2003). The systematics of chlorine, fluorine, and water in Izu arc front volcanic rocks: Implications for volatile recycling in subduction zones. *Geochimica et Cosmochimica Acta* **67**, 4179–4203.

Streck, M. J., Leeman, W. P. & Chesley, J. (2007). High-magnesian andesite from Mount Shasta: A product of magma mixing and contamination, not a primitive mantle melt. *Geology* **35**, 351–354.

Streck, M. J., Leeman, W. P. & Chesley, J. (2008). Reply to the comment on 'High-magnesian andesites from Mount Shasta: a product of magma mixing and contamination, not a primitive melt' Streck, M. J., Leeman, W. P., Chelsey, J. *Geology* **35**, e147–e148.

Sugawara, T. (2000). Empirical relationships between temperature, pressure, and MgO content in olivine and pyroxene saturated liquid. *Journal of Geophysical Research* **105**, 8457–8472.

Tatsumi, Y. & Eggins, S. (1995). *Subduction Zone Magmatism*. Oxford: Blackwell Science.

Toplis, M. J. (2005). The thermodynamics of iron and magnesium partitioning between olivine and liquid: criteria for assessing and predicting equilibrium in natural and experimental systems. *Contributions to Mineralogy and Petrology* **149**, 22–39.

Vigouroux, N., Wallace, P. J. & Kent, A. J. R. (2008). Volatiles in high-K magmas from the western Trans-Mexican Volcanic Belt: evidence for fluid fluxing and extreme enrichment of the mantle wedge by subduction processes. *Journal of Petrology* **49**, 1589–1618.

Wade, J. A., Plank, T., Melson, W. G., Soto, G. J. & Hauri, E. H. (2006). The volatile content of magmas from Arenal volcano, Costa Rica. *Journal of Volcanology and Geothermal Research* **157**, 94–120.

Walker, J. A., Roggensack, K., Patino, L. C., Cameron, B. I. & Matias, O. (2003). The water and trace element contents of melt inclusions across an active subduction zone. *Contributions to Mineralogy and Petrology* **146**, 62–77.

Wallace, P. J. (2005). Volatiles in subduction zone magmas: concentrations and fluxes based on melt inclusion and volcanic gas data. *Journal of Volcanology and Geothermal Research* **140**, 217–240.

Watson, J. B., Sneeringer, M. A. & Ross, A. (1982). Diffusion of dissolved carbonate in magmas: experimental results and applications. *Earth and Planetary Science Letters* **61**, 346–358.

Webster, J. D. (2004). The exsolution of magmatic hydrosaline chloride liquids. *Chemical Geology* **210**, 33–48.

Webster, J. D., Tappen, C. M. & Mandeville, C. W. (2009). Partitioning behavior of chlorine and fluorine in the system apatite–melt–fluid. II: Felsic silicate systems at 200 MPa. *Geochimica et Cosmochimica Acta* **73**, 559–581.

Williams, H. (1932*a*). Geology of the Lassen Volcanic National Park, California. *California University, Department of Geology Scientific Bulletin* **21**, 195–385.

Williams, H. (1932*b*). Mount Shasta, a Cascade volcano. *Journal of Geology* **45**, 417–429.

Williams, H. (1934). Mount Shasta, California. *Zeitschrift für Vulkanologie* **15**, 225–253.

Williams, H. (1949). *Geology of Macdoel quadrangle (California). Californian Division of Mines Bulletin* **151**.

Williams, L. B., Hervig, R. L., Holloway, J. R. & Hutcheon, I. (2001). Boron isotope geochemistry during diagenesis. Part I. Experimental determination of fractionation during illitization of smectite. *Geochimica et Cosmochimica Acta* **65**, 1769–1782.

Wilson, D. S. (1988). Tectonic history of the Juan de Fuca ridge over the last 40 Million years. *Journal of Geophysical Research* **93**.